Available online at www.sciencedirect.com
SCIENCE DIRECT®
Comput. Methods Appl. Mech. Engrg. 192 (2003) 47–76
Computer methods in applied mechanics and engineering
www.elsevier.com/locate/cma

Numerical methods for elliptic partial differential equations with rapidly oscillating coefficients

C. Conca [a,*], S. Natesan [b]

[a] Departamento de Ingeniería Matemática, Facultad de Ciencias Físicas y Matemáticas, Universidad de Chile, and Centro de Modelamiento Matemático, UMR 2071 CNRS-UChile, Casilla 170/3, Correo 3, Santiago, Chile
[b] Centro de Modelamiento Matemático, UMR 2071 CNRS-UChile, Casilla 170/3, Correo 3, Santiago, Chile

Received 7 November 2001; received in revised form 10 May 2002

Abstract

This paper presents two methods for the numerical solution of the classical homogenization problem of elliptic operators with periodically oscillating coefficients. The numerical solution of such problems is difficult because of the presence of rapidly oscillating coefficients. The first method based on the classical one which consists of the homogenized solution, the first- and second-order correctors, whereas the second one is based on the Bloch wave approach. Further, for the calculation of the homogenized coefficients and some auxiliary functions involved in this method, we applied both methods and compared their accuracies. The Bloch approximation consists in determining an oscillating integral, numerically. The Bloch method provides a better approximation to the exact solution than the classical first-order corrector term in the smooth coefficients case. Moreover, we provided Taylor approximations for the Bloch approximation function and implemented it numerically. In order to show the efficiency of these methods, exhaustive numerical examples in both one and two-dimensional cases are presented.

Keywords: Homogenization; Bloch waves; Periodic structures; Numerical solution of differential equations; Correctors

1. Introduction

Multi-scale problems in science and engineering are often described by partial differential equations (PDEs) with highly oscillating coefficients. Typical examples include flows in porous media, and turbulent transport problems. A complete analysis of these problems is extremely difficult. For example, the difficulty in analyzing ground water transport is mainly caused by the heterogeneity of subsurface formations spanning over many scales [3]. The heterogeneity is often represented by the multi-scale fluctuations in the permeability of the media. For composite materials, the dispersed phases (particles or fibers), which may be randomly distributed in the matrix give rise to fluctuations in the thermal or electrical conductivity; moreover, the conductivity is usually discontinuous across the phase boundaries. In turbulent transport

* Corresponding author.
E-mail addresses: cconca@dim.uchile.cl (C. Conca), natesan@dim.uchile.cl (S. Natesan).

0045-7825/03/$ - see front matter
PII: S0045-7825(02)00500-5

problems, the convective velocity field fluctuates randomly and contains many scales depending on the Reynolds number of the flow.

A direct numerical solution of the multiple scale problems is difficult even with modern supercomputers. The major difficulty of direct solutions is the scale of computation. For example, the numerical difficulties arising in the ground water simulation has been explained in [13]. In [7], the authors provided the details about the mixture of composite materials and the torsion of fiber-reinforced bars and their numerical simulations. Moreover, from an engineering perspective it is often sufficient to predict the macroscopic properties of the multiple-scale systems, such as the effective conductivity, elastic moduli, permeability, and eddy diffusivity. Therefore, it is desirable to develop a method that captures the small scale effect on the large scales, but which does not require resolving all the small scale features. For further applications of homogenization theory in physics and mechanics one may refer to Sánchez-Palencia [19].

For a nice introduction to homogenization, the reader is referred to the book of Bensoussan et al. [4]. The main result conveys that the (weak) limit of such solutions resolves a suitable boundary value problem which has constant coefficients that represent what is known as homogenized medium. There are many ways to obtain the homogenized coefficients and there is a vast body of work in the literature which justifies the limiting process. In [4], they used the method of multiple scale expansion to homogenization and their technique is the easiest way to obtain the homogenized medium.

Conca and Vanninathan [12] gave a new proof of convergence using Bloch wave decomposition. Further, they offered a non-traditional way of calculating the homogenized coefficients and more precisely, they proved that the classical homogenized matrix coincides with one-half of the Hessian of the first (minimum) Bloch eigenvalue at the origin. In a more recent paper [10], they introduced what they called the *Bloch approximation* function θ^ε to the solution u^ε of the original problem. This function provides a sharp approximation in the sense that it contains implicitly both the homogenized solution and the classical first-order corrector which were first obtained by Bensoussan et al. [4] by using a two-scale asymptotic expansion for the solution. It is worth emphasizing that in the case of smooth coefficients, θ^ε also contains the classical second-order corrector (see Theorem 1.11 in [10]). Further we would like to cite a recent work [1], in which the Bloch–Floquet approach is used to provide new homogenization results and handles the boundary layer terms for frequency-dependent problems.

In [8], the author studied the homogenization of a diffusion equation with drift. In order to study the homogenization of an eigenvalue problem, he introduced a family of θ-exponential periodic problems with a real exponent θ. When θ is purely imaginary one can encounter the Bloch waves carried out in [11] which will be implemented here numerically for the approximation. More details about the application of these types of problems in neutronic models may be found in the book of Planchard [18]. Kesavan [14] and Vanninathan [20] studied the behavior of the spectrum of elliptic differential operators under the homogenization process and predicted that the same operator which serves to homogenize the corresponding static problem works well for the eigenvalue problem also. Further these authors studied the effect of correctors. To determine some auxiliary functions involved in these methods (the so-called local periodic functions denoted by χ_k) which are used for the calculation of the homogenized coefficients in the classical sense, one can use the projection idea introduced here. And in addition, it is more convenient to use Bloch waves for the determination of the homogenized coefficients and χ_k.

To solve elliptic PDEs with rapidly oscillating coefficients Avellaneda et al. [2] applied finite difference method. Hou and Wu [13] introduced multi-scale finite element method for these types of problems. In [16], the authors proposed a p-finite element method in order to approximate the solution numerically in the one-dimensional case using a representation formula as given in [17].

Here, we obtain the numerical solution of the above mentioned problem by the classical way which combines the homogenized solution, the first- and second-order classical correctors and by the Bloch approximation function θ^ε. Our main goal is to carry out a comparative analysis between the classical and Bloch wave approach.

It is well known that in the classical method, one is led to solve numerically several periodic elliptic boundary value problems in the representative cell $Y =]0, 2\pi[^N$. The periodic boundary conditions in these problems will be treated by using the conjugate gradient algorithm with projection. That is, we solve the corresponding linear system by an iterative method and at each iteration we project the solution in such a way that for the grid points on the boundary we take the average of the value on the opposite faces. Then, one has to determine the homogenized coefficients and solve the homogenized equation. Also, we determine the first- and second-order periodic correctors in order to get a more accurate numerical approximation. Recall that by adding the first-order correctors to the homogenized solution yields an approximation in the energy norm for all sufficiently small ε. The second-order correctors provide an error estimate in the energy norm of order $O(\varepsilon)$.

To find the so-called Bloch waves one has to obtain an accurate approximation of a parameterized family of spectral problems in Y with a generalized periodic boundary condition. The main difficulty here is the numerical implementation of these generalized periodic boundary conditions. This is done by using the projection idea as above. But, here the projection includes exponential complex weighted average between the values on opposite faces. The details are given in Section 3.2. After discretization, each of these spectral problems reduce to a generalized eigenvalue problem of the Sylvester's type which can be solved numerically by standard algorithms. In order to find the homogenized coefficients, a fourth-order finite difference formula is used to obtain the Hessian of the first Bloch eigenvalue at the origin. This involves the computation of the first eigenvalue in a small ad hoc grid around the origin. To determine the function θ^ε we have to calculate the first (minimum) Bloch eigenvector in a small neighborhood of the origin and then apply a quadrature formula to approximate the integral numerically. The calculation of the first eigenvalue and eigenvector is independent at each point of the dual cell $Y' = [-1/2, 1/2[^N$ (Brillouin zone) which opens the door to utilize parallel computers.

In addition, it is known that the first Bloch mode $\phi_1(\cdot;\eta)$ is an analytic function of the Bloch variable η (for small η) and one can therefore expand it in a Taylor series around the origin. Using this expansion in the definition of θ^ε one can obtain some approximations for θ^ε which in its turn is an approximation of the exact solution u^ε, too. Here, we have obtained the first- and second-order approximations, and the numerical calculation of these terms are slightly simpler than the one of θ^ε.

To conclude our comparative analysis between the classical and Bloch methods for the homogenized coefficients, and the determination of χ_k, we applied it to several two-dimensional test problems. Also, we have showed the effects of first- and second-order correctors. From these examples one can justify the theoretical results as well as the accuracy of the method. In order to show the efficiency of the Bloch approximation function θ^ε over the classical first-order corrector, we consider continuous and discontinuous coefficients problem in one-dimension. Finally, for the same examples, we have applied the Taylor approximations of θ^ε and showed its accuracy. The computational results are presented in the forms of tables and figures.

The rest of the paper is organized as follows. Some theoretical results are given in Section 2. Section 3 deals with the computation of homogenized coefficients by classical and Bloch methods. Computation of the classical correctors are presented in Section 4. The numerical implementation and Taylor approximations of the Bloch approximation function θ^ε are given in Section 5. Numerical experiments are presented in Section 6.

2. Theoretical results

Consider the operator

$$A \stackrel{\text{def}}{=} -\frac{\partial}{\partial y_k}\left(a_{k\ell}(y)\frac{\partial}{\partial y_\ell}\right), \quad y \in \mathbb{R}^N, \tag{2.1}$$

where the coefficients satisfy

$$\begin{cases} a_{k\ell} \in L^{\infty}_{\#}(Y), \text{ where } Y =]0, 2\pi[^N, \text{ i.e., each } a_{k\ell} \text{ is a} \\ Y\text{-periodic bounded measurable function defined on } \mathbb{R}^N, \text{ and} \\ \exists \alpha > 0 \text{ such that } a_{k\ell}(y)\eta_k\eta_\ell \geqslant \alpha|\eta|^2, \ \forall \eta \in \mathbb{R}^N, \ \ y \in Y \text{ a.e.}, \\ a_{k\ell} = a_{\ell k} \ \forall k, \ell = 1, \ldots, N. \end{cases} \tag{2.2}$$

For each $\varepsilon > 0$, we also consider the operator A^ε where

$$A^\varepsilon \stackrel{\text{def}}{=} -\frac{\partial}{\partial x_k}\left(a^\varepsilon_{k\ell}(x)\frac{\partial}{\partial x_\ell}\right) \quad \text{with } a^\varepsilon_{k\ell}(x) = a_{k\ell}\left(\frac{x}{\varepsilon}\right), \ \ x \in \mathbb{R}^N. \tag{2.3}$$

In homogenization theory, it is usual to refer to x and y the slow and the fast variables respectively. They are related by $y = x/\varepsilon$. Associated with A^ε, let us consider the following boundary-value problem

$$A^\varepsilon u^\varepsilon = f \text{ in } \Omega, \quad u^\varepsilon \in H^1_0(\Omega), \tag{2.4}$$

which is posed in an arbitrary bounded domain $\Omega \in \mathbb{R}^N$ and f is a given element in $L^2(\Omega)$. The boundary of Ω is denoted by Γ. It is classical that the above problem admits one and only one solution.

Bensoussan et al. [4] obtained an asymptotic expansion for the solution of (2.4) of the following form:

$$u^\varepsilon(x) = u^*(x) + \varepsilon\left\{\chi_k(y)\frac{\partial u^*}{\partial x_k}(x) + \tilde{u}_1(x)\right\} + \varepsilon^2\left\{\chi_{k\ell}(y)\frac{\partial^2 u^*}{\partial x_k \partial x_\ell}(x) + \chi_\ell(y)\frac{\partial \tilde{u}_1}{\partial x_\ell}(x) + \tilde{u}_2(x)\right\} + \cdots \tag{2.5}$$

Here, χ_k is the unique solution of the cell problem

$$\begin{cases} A\chi_k = \dfrac{\partial a_{k\ell}}{\partial y_\ell} \quad \text{in } \mathbb{R}^N, \\ \chi_k \in H^1_{\#}(Y), \mathscr{M}_Y(\chi_k) \stackrel{\text{def}}{=} \frac{1}{|Y|}\int_Y \chi_k \, \mathrm{d}y = 0. \end{cases} \tag{2.6}$$

The function $\chi_{k\ell}$ is characterized as the unique solution of

$$\begin{cases} A\chi_{k\ell} = a_{k\ell} + a_{km}\dfrac{\partial \chi_\ell}{\partial y_m} - \dfrac{\partial}{\partial y_m}(a_{mk}\chi_\ell) - \mathscr{M}_Y(a_{k\ell}) - \mathscr{M}_Y\left(a_{km}\dfrac{\partial \chi_\ell}{\partial y_m}\right) \quad \text{in } \mathbb{R}^N, \\ \chi_{k\ell} \in H^1_{\#}(Y), \quad \mathscr{M}_Y(\chi_{k\ell}) = 0. \end{cases} \tag{2.7}$$

The first term in (2.5) satisfies the homogenized equation

$$\begin{cases} A^* u^* \stackrel{\text{def}}{=} -q_{k\ell}\dfrac{\partial^2 u^*}{\partial x_k \partial x_\ell} = f \quad \text{in } \Omega, \\ u^* \in H^1_0(\Omega), \end{cases} \tag{2.8}$$

where the homogenized coefficients $q_{k\ell}$ are given by

$$q_{k\ell} = \mathscr{M}_Y\left(a_{k\ell} + a_{km}\frac{\partial \chi_\ell}{\partial y_m}\right) \quad \forall k, \ell = 1, \ldots, N. \tag{2.9}$$

The above method also proves that $\tilde{u}_1(x), \tilde{u}_2(x), \ldots$ are independent of ε and satisfy equations of the type $A^*\tilde{u}_j = \tilde{g}_j$ in $\mathbb{R}^N$, where, for instance, $\tilde{g}_1(x) = b_{jk\ell}(\partial^3 u^*/\partial x_j \partial x_k \partial x_\ell)(x)$, where $b_{jk\ell}$ are constants:

$$b_{jk\ell} = \mathscr{M}_Y\left(a_{jm}\frac{\partial \chi_{k\ell}}{\partial y_m} + a_{k\ell}\chi_j\right) \quad \forall j, k, \ell = 1, \ldots, N.$$

In the present paper, we also consider the case of the whole space $\Omega = \mathbb{R}^N$. It is therefore natural to replace the operator A^ε by $(A^\varepsilon + I)$. In that case, if w^ε satisfies

$$\begin{cases} (A^\varepsilon + I)w^\varepsilon = g & \text{in } \mathbb{R}^N, \\ w^\varepsilon \rightharpoonup w^* & \text{in } H^1(\mathbb{R}^N)\text{-weak}, \end{cases} \tag{2.10}$$

where g is a given function in $L^2(\mathbb{R}^N)$, then it can be proved (see Lemma 6.1 of [10]) that

$$w^\varepsilon \to w^* \quad \text{in } L^2(\mathbb{R}^N)\text{-strong}. \tag{2.11}$$

In view of the above result, there is no concentration of L^2-energy at infinity and therefore, we will consider throughout this paper a sequence u^ε in $H^1(\mathbb{R}^N)$ and a function f in $L^2(\mathbb{R}^N)$ satisfying

$$\begin{cases} A^\varepsilon u^\varepsilon = f & \text{in } \mathbb{R}^N, \\ u^\varepsilon \rightharpoonup u^* & \text{in } H^1(\mathbb{R}^N)\text{-weak}, \\ u^\varepsilon \to u^* & \text{in } L^2(\mathbb{R}^N)\text{-strong}. \end{cases} \tag{2.12}$$

Conca and Vanninathan [12] gave an alternative formula for the homogenized coefficients as defined in (2.9). They have studied the spectral resolution of A in $L^2(\mathbb{R}^N)$. For this, they used the classical method of Bloch [5] which consists of introducing a family of spectral problems parametrized by $\eta \in \mathbb{R}^N$: find $\lambda = \lambda(\eta) \in \mathbb{R}$ and $\psi = \psi(y;\eta)$ (not identically zero) such that

$$\begin{cases} A\psi(\cdot;\eta) = \lambda(\eta)\psi(\cdot;\eta) \quad \text{in } \mathbb{R}^N, \ \ \psi(\cdot;\eta) \text{ is } (\eta;Y)\text{-periodic, i.e.,} \\ \psi(y + 2\pi m;\eta) = \mathrm{e}^{2\pi \mathrm{i} m\cdot\eta}\psi(y;\eta) \quad \forall m \in \mathbb{Z}^N, \ \ y \in \mathbb{R}^N. \end{cases} \tag{2.13}$$

By using the following transformation

$$\begin{cases} \psi(y;\eta) = \mathrm{e}^{\mathrm{i}\eta\cdot y}\phi(y;\eta), \\ \phi(\cdot;\eta) \quad \text{is } Y\text{-periodic}, \end{cases} \tag{2.14}$$

the problem (2.13) becomes

$$A(\eta)\phi = \lambda\phi \quad \text{in } \mathbb{R}^N, \ \ \phi \text{ is } Y\text{-periodic},$$

where the operator $A(\eta)$ is defined by

$$A(\eta) \stackrel{\text{def}}{=} -\left(\frac{\partial}{\partial y_k} + \mathrm{i}\eta_k\right)\left(a_{k\ell}(y)\left(\frac{\partial}{\partial y_\ell} + \mathrm{i}\eta_\ell\right)\right)$$

and it is referred to as the shifted operator. It is clear from (2.13) that the (η, Y) periodicity condition is unaltered if we replace η by $(\eta + q)$ with $q \in \mathbb{Z}^N$ and η can therefore be confined to the *dual cell* $Y' = [-1/2, 1/2[^N$.

It is well known that, due to ellipticity and symmetry hypothesis, the above problem admits a unique sequence of eigenvalues in the following spaces

$$L^2_\#(Y) = \{\phi \in L^2_{\text{loc}}(\mathbb{R}^N) | \phi \text{ is } Y\text{-periodic}\},$$
$$H^1_\#(Y) = \left\{\phi \in L^2_\#(Y) \middle| \frac{\partial\phi}{\partial y_k} \in L^2_\#(Y) \ \forall k = 1, \ldots, N\right\}.$$

They have the following properties

$$\begin{cases} 0 \leqslant \lambda_1(\eta) \leqslant \cdots \leqslant \lambda_m(\eta) \leqslant \cdots \to \infty, \\ \{\phi_m(\cdot;\eta)\}_{m=1}^\infty \text{ forms an orthonormal basis in } L^2_\#(Y). \end{cases}$$

In the literature, $\{\lambda_m(\eta)\}_{m \geqslant 1}$ are referred to as Bloch eigenvalues and $\{\phi_m(\cdot;\eta)\}_{m \geqslant 1}$ as Bloch eigenvectors or Bloch waves.

The following theorem gives the relation between the above eigenvalues and the homogenized coefficients.

Theorem 2.1. [12] *We assume that $a_{k\ell}$ satisfy* (2.2). *Then there exists $\delta > 0$ such that the first eigenvalue $\lambda_1(\eta)$ is an analytic function on $B_\delta \overset{\text{def}}{=} \{\eta | \, |\eta| < \delta\}$, and there is a choice of the first eigenvector $\phi_1(y;\eta)$ satisfying*

$$\begin{cases} \eta \to \phi_1(\cdot;\eta) \in H^1_{\#}(Y) \text{ is analytic on } B_\delta, \\ \phi_1(y;0) = p^{(0)}\left(= |Y|^{-1/2} = \frac{1}{(2\pi)^{N/2}}\right). \end{cases}$$

Moreover, we have the relations

$$\lambda_1(0) = 0, \quad D_k\lambda_1(0) \overset{\text{def}}{=} \frac{\partial \lambda_1}{\partial \eta_k}(0) = 0, \qquad \forall k = 1, \ldots, N.$$

Further, the Hessian of λ_1 at $\eta = 0$ is given by

$$\frac{1}{2} D^2_{k\ell}\lambda_1(0) \overset{\text{def}}{=} \frac{1}{2} \frac{\partial^2 \lambda_1}{\partial \eta_k \, \partial \eta_\ell}(0) = q_{k\ell} \quad \forall k, \ell = 1, \ldots, N. \tag{2.15}$$

The derivatives of the first Bloch mode can also be calculated and they are as follows:

$$\frac{\partial \phi_1}{\partial \eta_k}(y;0) = \mathrm{i}|Y|^{-1/2}\chi_k(y) \quad \forall k = 1, \ldots, N. \tag{2.16}$$

Let us consider the sequence u^ε satisfying the hypotheses as given in (2.12). The Bloch approximation of u^ε is defined by the following formula:

$$\theta^\varepsilon(x) \overset{\text{def}}{=} \frac{1}{\varepsilon^N} \int_{Y'} \hat{u}^*\left(\frac{\eta}{\varepsilon}\right) \mathrm{e}^{\mathrm{i}(x/\varepsilon)\cdot\eta} \phi_1\left(\frac{x}{\varepsilon};\eta\right) \mathrm{d}\eta, \quad x \in \mathbb{R}^N, \tag{2.17}$$

where $\hat{u}^*$ is the classical Fourier transform of the homogenized solution u^*, and ϕ_1 is the first Bloch mode.

We conclude this section with the following two theorems of [10] which provide an estimate for the difference between θ^ε, u^ε and the classical first- and second-order corrector terms.

Theorem 2.2. *Assume that the coefficients $a_{k\ell}$ satisfy* (2.2). *Let u^ε be the sequence introduced in* (2.12). *Then if $f \in L^2(\mathbb{R}^N)$, we have*

$$(u^\varepsilon - \theta^\varepsilon) \to 0 \quad \text{in } H^1(\mathbb{R}^N). \tag{2.18}$$

Furthermore, we have the estimate

$$|u^\varepsilon - \theta^\varepsilon|_{H^1(\mathbb{R}^N)} \leqslant c\varepsilon \|f\|_{L^2(\mathbb{R}^N)}. \tag{2.19}$$

Moreover, because of the analyticity of $\phi_1(\cdot;\eta)$ for $|\eta| \leqslant \delta$ and assuming smooth coefficients $a_{kl}(\cdot)$ in the operator A (which ensure the smoothness of the auxiliary functions χ_k, χ_{kl} in (ii) and (iii) of Theorem 2.3), we can expand it and this give rises to an asymptotic expansion of θ^ε which is as follows:

$$\theta^\varepsilon(x) = u^*(x) + \varepsilon\chi_k\left(\frac{x}{\varepsilon}\right)\frac{\partial u^*}{\partial x_k}(x) - \varepsilon^2\left(\chi_{k\ell}\left(\frac{x}{\varepsilon}\right) + \beta_{k\ell}\right)\frac{\partial^2 u^*}{\partial x_k \, \partial x_\ell}(x) + \cdots,$$

where β_{kl} are real constants (for details, see statement (iii) in Theorem 2.3 below).

Theorem 2.3. *Assume that the hypotheses of Theorem* 2.2 *hold. Then the following statements hold true.*

(i) *If $u^* \in H^1(\mathbb{R}^N)$, then*

$$\|\theta^\varepsilon - u^*\|_{L^2(\mathbb{R}^N)} \leqslant c\varepsilon \|u^*\|_{H^1(\mathbb{R}^N)}.$$

(ii) *If* $f \in L^2(\mathbb{R}^N)$ *and* $\chi_k \in W^{1,\infty}_{\#}(Y)$ *where* χ_k *is the solution of* (2.6) *and* $\chi^\varepsilon_k(x) = \chi_k(x/\varepsilon)$, *then we have*

$$\left\| \theta^\varepsilon - u^* - \varepsilon \chi^\varepsilon_k \frac{\partial u^*}{\partial x_k} \right\|_{H^1(\mathbb{R}^N)} \leqslant c\varepsilon \|f\|_{L^2(\mathbb{R}^N)}.$$

(iii) *If* $f \in H^1(\mathbb{R}^N)$ *and* χ_k, $\chi_{k\ell} \in W^{1,\infty}_{\#}(Y)$, *then*

$$\left\| \theta^\varepsilon - u^* - \varepsilon \chi^\varepsilon_k \frac{\partial u^*}{\partial x_k} + \varepsilon^2 \left(\chi^\varepsilon_{k\ell} + \beta_{k\ell}\right) \frac{\partial^2 u^*}{\partial x_k \partial x_\ell} \right\|_{H^1(\mathbb{R}^N)} \leqslant c\varepsilon^2 \|f\|_{H^1(\mathbb{R}^N)},$$

where $\chi^\varepsilon_{k\ell}(x) = \chi_{k\ell}(x/\varepsilon)$, *and* β_{kl} *are constants given by*

$$\beta_{k\ell} = \frac{1}{2!} \frac{1}{|Y|} \int_Y \chi_\ell \chi_k \, \mathrm{d}y.$$

3. Computation of the homogenized coefficients

3.1. Classical method

In this section, we determine the homogenized coefficients using the classical formula as given in (2.9). Here, we consider the two-dimensional case ($N = 2$). In all our test problems, we will distinguish in Y two different regions Y_0 and Y_1, where the coefficients $a_{k\ell}$ take different values. In order to solve problem (2.6) which gives the functions χ_k, we use the finite element method with Lagrange finite elements of degree one on triangles. Though the computation does not require a fine mesh, we use a fine mesh in Y because the homogenized coefficients $q_{k\ell}$ are obtained from the first derivatives of the functions χ_k. Here, one should make sure that the triangulation is made in such a way that the discontinuities of the coefficients $a_{k\ell}$ coincide with the sides of the triangles.

The variational formulation of (2.6) is to seek $\chi_k \in V_{\#} \stackrel{\text{def}}{=} H^1_{\#}(Y)$, such that

$$a(\chi_k, \zeta) = f(\zeta) \quad \forall \zeta \in V_{\#}, \tag{3.1}$$

where

$$a(\chi_k, \zeta) = \int_Y a_{k\ell} \frac{\partial \chi_k}{\partial y_\ell} \frac{\partial \zeta}{\partial y_k} \mathrm{d}y \quad \text{and} \quad f(\zeta) = \int_Y a_{k\ell} \frac{\partial \zeta}{\partial y_\ell} \mathrm{d}y.$$

It is easy to see that the bilinear form $a(\cdot,\cdot)$ is elliptic and continuous. A finite element method is obtained by restricting the weak formulation (3.1) to a finite dimensional subspace of $V_{\#}$. For $0 \leqslant h \leqslant 1$, let $\mathscr{T}_h$ be a periodic partition of Y by a collection of triangles T with diameter less than or equal to h, such that

$$\overline{Y} = \bigcup_{T \in \mathscr{T}_h} T.$$

Let us define the discretization space V_h as

$$V_h \stackrel{\text{def}}{=} \{\phi^h \in \mathscr{C}^0(\overline{Y}) : \phi^h|_T \in \mathscr{P}_1(T),\ \forall T \in \mathscr{T}_h\},$$

where $\mathscr{P}_1(T)$ is the space of polynomials of degree at most one. As usual, a basis for V_h is defined by $\{\phi_i,\ i = 1, \ldots, N_h\}$; N_h being the number of nodes of the partition. Let $(x_j, y_j) \in \overline{Y} (j = 1, \ldots, N_h)$ be a grid point. In addition, we require $\phi_i(x_j, y_j) = \delta_{ij}$. Consider the following discretization subspace $V_{\#h}$ of $V_{\#}$ such that

$$V_{\#h} \stackrel{\text{def}}{=} \{\phi^h \in V_h | \phi^h \text{ is } Y\text{-periodic}\}.$$

In the following, we study the approximate solution $\chi_k^h \in V_{\#h}$ of (3.1), which is defined to be the unique solution of the discrete problem

$$a(\chi_k^h, \zeta^h) = f(\zeta^h) \quad \forall \zeta^h \in V_{\#h}. \tag{3.2}$$

It is difficult to use direct methods to solve the linear system (3.2) because the periodicity conditions disturb the band structure of the matrix. Bourgat used the over relaxation method with an optimal parameter to solve the discretized system in [6]. The main drawback of this method is the selection of the optimal parameter to obtain faster convergence. To overcome this difficulty, here, we apply the conjugate gradient method to solve the linear system. In addition, theoretically, the conjugate gradient algorithm converges to the exact solution in at most n iterations for an $n \times n$ system. The periodic boundary conditions are treated by projecting the numerical solution at each iteration in the space of periodic functions. In other words, the corresponding linear system is solved by an iterative method and the solution is projected in such a way that for the grid points on the boundary the average of the values on the opposite faces is used as the common value.

More precisely, let us express χ_k^h as a linear combination of the basis functions, i.e,

$$\chi_k^h(x,y) = \sum_{i=1}^{N_h} U_i \phi_i(x,y), \tag{3.3}$$

where the coefficients U_i, for $i = 1, \ldots, N_h$ are to be determined.

Let us denote the discrete interior and discrete boundary of Y respectively by

$$\text{Int}\, Y_h = \{(x_j, y_j) \in \overline{Y} | 0 < x_j < 2\pi, 0 < y_j < 2\pi\},$$
$$\partial Y_h = \{(x_j, y_j) \in \overline{Y} | x_j = 0 \text{ or } 2\pi \text{ and } y_j = 0 \text{ or } 2\pi\}.$$

If $(x_j, y_j) \in \partial Y_h$, we shall denote the corresponding opposite grid point by $(x_{j'}, y_{j'})$ which is well defined by virtue of periodic triangulation. We introduce the projection operator $P_h : V_h \to V_{\#h}$ as follows:

$$P_h(v_h) = v_{\#h},$$

where

$$v_{\#h}(x_j, y_j) = \begin{cases} v_h(x_j, y_j) & \text{if } (x_j, y_j) \in \text{Int}\, Y_h, \\ \frac{1}{2}[v_h(x_j, y_j) + v_h(x_{j'}, y_{j'})] & \text{if } (x_j, y_j) \in \partial Y_h. \end{cases}$$

We will apply the above projection operator at each iteration of the conjugate gradient algorithm. From the numerical examples provided in Section 6, one can see that this modified conjugate gradient algorithm converges within a finite number of iterations.

3.2. Bloch wave method

In order to obtain the homogenized coefficients by the Bloch wave method and to determine the Bloch approximation function θ^ε, we have to solve the elliptic problem (2.13) for each $\eta \in Y' = [-1/2, 1/2[^N$. Thus, let us fix $\eta \in Y'$ and consider the following generalized periodic eigenvalue problem

$$\begin{cases} -\dfrac{\partial}{\partial y_k}\left(a_{k\ell}(y)\dfrac{\partial}{\partial y_\ell}\right)\psi(\cdot;\eta) = \lambda(\eta)\psi(\cdot;\eta) & \text{in } Y, \\ \psi(\cdot;\eta) \text{ is } (\eta, Y)\text{-periodic.} \end{cases} \tag{3.4}$$

To obtain a weak formulation of (3.4), we introduce the following space of (η, Y)-periodic functions

$$H^1_{\#}(\eta; Y) = \left\{ \psi \in L^2_{\#}(\eta; Y) \,\middle|\, \frac{\partial \psi}{\partial y_k} \in L^2_{\#}(\eta; Y) \ \forall k = 1, \ldots, N \right\},$$

where $L^2_{\#}(\eta; Y)$ is the space of all $L^2_{\mathrm{loc}}(\mathbb{R}^N)$-functions which are $(\eta; Y)$-periodic.

The weak formulation of (3.4) is to find $\psi \in W_{\#} \overset{\mathrm{def}}{=} H^1_{\#}(\eta; Y)$, such that

$$a(\psi, \zeta) = \lambda(\eta) g(\zeta) \quad \forall \zeta \in W_{\#}, \tag{3.5}$$

where

$$g(\zeta) = \int_Y \psi \zeta \, \mathrm{d}y.$$

Let us define the finite dimensional subspace $W_{\#h}$ of $W_{\#}$ by

$$W_{\#h} = \{ \phi^h \in V_h | \phi^h \text{ is } (\eta; Y)\text{-periodic} \}.$$

The finite element approximation of (3.5) consists in finding $\psi^h \in W_{\#h}$ such that

$$a(\psi^h, \zeta^h) = \lambda(\eta) g(\zeta^h) \quad \forall \zeta^h \in W_{\#h}. \tag{3.6}$$

The (η, Y)-periodic projection operator $P^\eta_h : V_h \to W_{\#h}$ is defined as

$$P^\eta_h(v_h) = w^\eta_{\#h},$$

where

$$w^\eta_{\#h}(x_j, y_j) = v_h(x_j, y_j) \quad \text{if } (x_j, y_j) \in \operatorname{Int} Y_h$$

and if (x_j, y_j) is on the boundary ∂Y_h, we shall distinguish the following cases:

$$w^\eta_{\#h}(0, y_j) = \mathrm{e}^{-2\pi \mathrm{i} \eta_1} w^\eta_{\#h}(2\pi, y_j) \overset{\mathrm{def}}{=} \tfrac{1}{2}[v_h(0, y_j) + \mathrm{e}^{-2\pi \mathrm{i} \eta_1} v_h(2\pi, y_j)] \tag{3.7}$$

and

$$w^\eta_{\#h}(x_j, 0) = \mathrm{e}^{-2\pi \mathrm{i} \eta_2} w^\eta_{\#h}(x_j, 2\pi) \overset{\mathrm{def}}{=} \tfrac{1}{2}[v_h(x_j, 0) + \mathrm{e}^{-2\pi \mathrm{i} \eta_2} v_h(x_j, 2\pi)]. \tag{3.8}$$

Observe that with this projection we have for the four corner points,

$$w^\eta_{\#h}(0, 0) = \tfrac{1}{4}[v_h(0, 0) + \mathrm{e}^{-2\pi \mathrm{i} \eta_1} v_h(2\pi, 0) + \mathrm{e}^{-2\pi \mathrm{i}(\eta_1 + \eta_2)} v_h(2\pi, 2\pi) + \mathrm{e}^{-2\pi \mathrm{i} \eta_2} v_h(0, 2\pi)]$$

and

$$\mathrm{e}^{-2\pi \mathrm{i} \eta_2} w^\eta_{\#h}(0, 2\pi) = \mathrm{e}^{-2\pi \mathrm{i} \eta_1} w^\eta_{\#h}(2\pi, 0) = \mathrm{e}^{-2\pi \mathrm{i}(\eta_1 + \eta_2)} w^\eta_{\#h}(2\pi, 2\pi) = w^\eta_{\#h}(0, 0).$$

For the sake of convenience, let us denote respectively by $\{v_i\}_{i=1}^{N_h}$ and $\{w_i\}_{i=1}^{N_{\#h}}$ the standard finite element basis of V_h and $W_{\#h}$. The approximate function ψ^h can be expressed in two different ways, say

$$\psi^h(x, y) = \sum_{i=1}^{N_{\#h}} T_i w_i(x, y) \quad \text{or} \quad \psi^h(x, y) = \sum_{i=1}^{N_h} S_i v_i(x, y).$$

Let Q be the $N_{\#h} \times N_h$ matrix representing the projection operator P^η_h. Therefore, one can write the problem (3.6) in the following equivalent form:

$$\begin{cases} \text{Find } S \in \mathbb{R}^{N_h}, \ \lambda^h(\eta) \in \mathbb{R}, \text{ such that} \\ AS = \lambda^h(\eta) BS \ \text{ and } \ Q^{\mathrm{t}} T = S, \end{cases} \tag{3.9}$$

where A and B are respectively the finite element matrices in the space V_h associated with $a(\cdot, \cdot)$ and $g(\cdot)$ as defined in (3.6). In its turn, (3.9) can be reduced to the following generalized eigenvalue problem of Sylvester's type:

$$\begin{cases} \text{Find } T \in \mathbb{R}^{N_{\#h}},\ \lambda^h(\eta) \in \mathbb{R}, \text{ such that} \\ CT = \lambda^h(\eta) DT, \end{cases} \tag{3.10}$$

where $C = QAQ^{\mathrm{t}}$ and $D = QBQ^{\mathrm{t}}$.

From a computational point of view, matrix Q need not be stored in the memory, since matrices C and D can be obtained respectively from matrices A and B by means of suitable elementary operations on rows and columns corresponding to the boundary grid points. These elementary operations are nothing but formulas (3.7) and (3.8) which define the (η, Y)-projection operator P_h^η in the case of boundary grid points.

In order to determine the homogenized coefficients, we have to find the first eigenvalue λ_1 of the above Sylvester's type problem in a small neighborhood of the origin in Y'. After finding λ_1 in a small ad hoc grid points around $(0,0)$, a fourth-order finite difference formula is used to calculate the second derivative of λ_1 at $\eta = (0,0)$ which provides the homogenized coefficients as given by (2.15).

4. Computation of classical first- and second-order correctors

This section deals with the computation of first- and second-order periodic correctors for the solution u^ε of (2.4). The idea behind introducing correctors is to look for terms (called *first-order correctors*) which when added to the homogenized solution u^* provide an approximation in the energy norm for all sufficiently small ε. *Second-order correctors* yield an error estimate in the energy norm of order $\mathrm{O}(\varepsilon)$. The central issue in the analysis of the first-order correctors is to obtain functions $u_1^\varepsilon \in H^1(\Omega)$ which can be easily constructed and have the following characteristic property

$$\|u^\varepsilon - u^* - \varepsilon u_1^\varepsilon\|_{H^1(\Omega)} \to 0 \quad \text{as } \varepsilon \to 0. \tag{4.1}$$

By definition, second-order correctors $u_2^\varepsilon \in H^1(\Omega)$ would enjoy the property

$$\|u^\varepsilon - u^* - \varepsilon u_1^\varepsilon - \varepsilon^2 u_2^\varepsilon\|_{H^1(\Omega)} \leqslant c\varepsilon^2. \tag{4.2}$$

However, as far as the author's knowledge goes existence of a second-order corrector satisfying such a general and sharp error estimate even in the case of smooth coefficients is not proved in the literature at least for a bounded domain. This may be due to the boundary layers effects arising from the boundary conditions. In the unbounded domain case $\Omega = \mathbb{R}^N$ or $\Omega = \mathbb{R}^N_+$ (the positive half-space) with constant coefficients, sharp error estimates are proved by Lions [15]. For the second-order corrector term given by the asymptotic expansion (2.5), Bourgat [6] suggests a rate of convergence in $\varepsilon^{3/2}$ (which is far from being optimal), but the proof is not provided.

Under suitable assumptions on the smoothness of the coefficients $a_{k\ell}$ and if $f \in L^2(\Omega)$, then the classical first-order corrector is defined by

$$u_1^\varepsilon(x) = \chi_k\left(\frac{x}{\varepsilon}\right)\frac{\partial u^*}{\partial x_k}(x). \tag{4.3}$$

Furthermore, it is also given that the principal second-order term in the expansion (2.5) has been classically considered a second-order corrector, we will denote it by

$$u_2^\varepsilon(x) = \chi_{k\ell}\left(\frac{x}{\varepsilon}\right)\frac{\partial^2 u^*}{\partial x_k x_\ell}(x). \tag{4.4}$$

The function $\chi_{k\ell}$ appeared in (4.4) is the solution of (2.7) which differs from (2.6) only in the right hand side. So, one can compute $\chi_{k\ell}$ in a similar way as used in the calculation of χ_k.

For computation of the derivatives $\partial u^*/\partial x_k$ and $\partial^2 u^*/\partial x_k \partial x_\ell$, which appear in the calculation of the first- and second-order correctors u_1^ε, u_2^ε a fine discretization of Ω is needed. Here, we use more number of

triangles in order to obtain a better approximation for the derivatives. If the triangles are not locally too different and if the right hand side function f in (2.8) is smooth, we can approximate $\partial u^*/\partial x_k$ at each node P by

$$\frac{\partial u^*}{\partial x_k}(P) \stackrel{\text{def}}{=} \frac{1}{N_V(P)} \sum_{T \in V(P)} \left[\frac{\partial u^*}{\partial x_k}\right]_T, \tag{4.5}$$

where $V(P)$ is the set of triangles for which P is a common vertex, $N_V(P)$ is the number of triangles of $V(P)$, $[\partial u^*/\partial x_k]_T$ is the value of the derivative $\partial u^*/\partial x_k$ on triangle T. If the triangles are locally too different, then the above interpolation rule can be generalized to a more consistent formula by weighting the sum (4.5) by the volume of the cells. Using twice the formula as given in (4.5) one can obtain an approximation for $\partial^2 u^*/\partial x_k \partial x_\ell$.

Remark 4.1. Here, we point out that χ_k and $\chi_{k\ell}$ have been computed only in the representative cell Y. But they are in $H^1_{\#}(Y)$, by periodicity one can extend it to the whole domain Ω in order to determine the values of χ_k and $\chi_{k\ell}$ in the computations of correctors u_1^ε and u_2^ε.

5. Numerical implementation of the Bloch approximation θ^ε

Here, in this section, we present the details of the numerical implementation of the Bloch approximation function θ^ε. In addition, we provide first- and second-order Taylor approximations for θ^ε which are easier to determine numerically than θ^ε and provides better approximations to the exact solution u^ε.

In the two-dimensional case, θ^ε as given in (2.17) can be rewritten in the following way:

$$\theta^\varepsilon(x) = \varepsilon^{-2} \int_{Y'} \hat{\boldsymbol{u}}^*\left(\frac{\eta}{\varepsilon}\right) \mathrm{e}^{\mathrm{i}(x/\varepsilon)\cdot\eta} \phi_1\left(\frac{x}{\varepsilon};\eta\right) \mathrm{d}\eta, \tag{5.1}$$

where ϕ_1 is the first (minimum) eigenvector of the Sylvester's type eigenvalue problem (3.10). In order to obtain $\hat{\boldsymbol{u}}^*(\eta/\varepsilon)$ explicitly, we shall write the homogenized equation in the Fourier space

$$q_{k\ell}\xi_k\xi_\ell \hat{\boldsymbol{u}}^*(\xi) + \hat{\boldsymbol{u}}^*(\xi) = \hat{\boldsymbol{f}}(\xi) \quad \forall\, \xi \in \mathbb{R}^2.$$

More precisely, we have

$$(q_{k\ell}\eta_k\eta_\ell + \varepsilon^2)\hat{\boldsymbol{u}}^*\left(\frac{\eta}{\varepsilon}\right) = \varepsilon^2 \hat{\boldsymbol{f}}\left(\frac{\eta}{\varepsilon}\right). \tag{5.2}$$

Using (5.2) in (5.1), we obtain

$$\theta^\varepsilon(x) = \int_{Y'} \frac{\hat{\boldsymbol{f}}\left(\frac{\eta}{\varepsilon}\right)}{(q_{k\ell}\eta_k\eta_\ell + \varepsilon^2)} \mathrm{e}^{\mathrm{i}x\cdot(\eta/\varepsilon)} \phi_1\left(\frac{x}{\varepsilon};\eta\right) \mathrm{d}\eta \quad \forall\, x \in \mathbb{R}^2. \tag{5.3}$$

We would like to recall that the first Bloch eigenvalue $\lambda_1(\eta)$ and the first Bloch eigenvector $\phi_1(\cdot,\eta)$ depend analytically on η in a small neighborhood B_δ of $\eta = 0$. To compute these two terms, we solve the generalized Sylvester's type eigenvalue problem (3.10) in a small ad hoc grid points around $(0,0)$ in $Y' = [-1/2, 1/2[$. The obtained eigenvectors $\psi_1(\cdot,\eta)$ are (η, Y)-periodic. By using the transformation as given in (2.14), we obtain the Y-periodic eigenvectors $\phi_1(\cdot,\eta)$. Further, we make the following normalizations on these eigenvectors $\phi_1(\cdot,\eta)$:

$$\|\phi_1(\cdot;\eta)\|_{L^2(Y)} = 1 \quad \forall\, \eta \in B_\delta,$$

$$\mathfrak{Im} \int_Y \phi_1(y;\eta)\, \mathrm{d}y = 0 \quad \forall\, \eta \in B_\delta.$$

From the eigenvalues $\lambda_1(\eta)$ we determine the homogenized coefficients as mentioned in Section 3.2. These Bloch eigenvalues and eigenvectors are independent of ε, as an outcome it is not necessary to compute these for each value of ε. In other words, the calculation is once for ever in the computation of $\theta^\varepsilon(x)$. Now, each term in the integrand of $\theta^\varepsilon(x)$ is known explicitly, by the use of a quadrature formula one can compute, in practice, the integral (5.3) numerically, here we apply the classical Simpson's rule.

In this paper, we have numerically determined θ^ε only in the one-dimensional case in Section 6.2.1. This is a first attempt to compare the Bloch method with the classical one and the authors are working on the numerical implementation of θ^ε in the two-dimensional case [9]. The numerical implementation of the Bloch method is not straightforward in the two-dimensional case, because the cell eigenvalue problems involved are much bigger than the one-dimensional case. This large-scale computations have some difficulties in the implementation not only in the determination of eigenvalues but also in the quadrature formula.

5.1. Taylor approximations of θ^ε

In this section, we propose two approximations for θ^ε based on Taylor series expansion for the first Bloch mode ϕ_1 with respect to η. To this end, we utilize the properties of ϕ_1 as stated in Theorem 2.1. Since ϕ_1 is an analytic function in the Bloch variable η, one can suggest to replace it in formula (5.3) by its linear affine and its quadratic approximations at $\eta = 0$. At a first glance this may seem to be little audacious since such approximations are only accurate in a small neighborhood of $\eta = 0$, where ϕ_1 is indeed analytic. However, it is well known (see [10]) that the contribution of the components of ϕ_1 for values of η far away from the origin are not important, i.e., they do not play any important role in the computation of the integral over Y'.

5.1.1. First-order approximation

More exactly, we propose the following linear affine approximation for θ^ε:

$$\tilde{\theta}^\varepsilon_{(1)}(x) = \int_{Y'} \frac{\hat{f}\left(\frac{\eta}{\varepsilon}\right)}{(q_{k\ell}\eta_k\eta_\ell + \varepsilon^2)} e^{i(x/\varepsilon)\cdot\eta} \left[\phi_1(\cdot;0) + \frac{\partial\phi_1}{\partial\eta_k}(\cdot;0)\eta_k\right] d\eta \quad \forall x \in \mathbb{R}^2. \tag{5.4}$$

If we use the explicit formulas for the first two terms in the right hand side of (5.4) given in Theorem 2.1, then we can rewrite $\tilde{\theta}^\varepsilon_{(1)}$ as follows:

$$\tilde{\theta}^\varepsilon_{(1)}(x) = \frac{1}{2\pi} \int_{Y'} \frac{\hat{f}\left(\frac{\eta}{\varepsilon}\right)}{(q_{k\ell}\eta_k\eta_\ell + \varepsilon^2)} e^{i(x/\varepsilon)\cdot\eta} \left[1 + i\chi_k\left(\frac{x}{\varepsilon}\right)\eta_k\right] d\eta \quad \forall x \in \mathbb{R}^2. \tag{5.5}$$

It is more easy to implement the above formula numerically than θ^ε because the auxiliary function χ_k is much easier to compute numerically than ϕ_1. The computation of χ_k can be done either by solving problem (2.6) directly or by evaluating the left hand side of (2.16) numerically.

5.1.2. Second-order approximation

The second-order approximation for the Bloch approximation function $\theta^\varepsilon(x)$ is given by

$$\tilde{\theta}^\varepsilon_{(2)}(x) = \int_{Y'} \frac{\hat{f}\left(\frac{\eta}{\varepsilon}\right)}{(q_{k\ell}\eta_k\eta_\ell + \varepsilon^2)} e^{i(x/\varepsilon)\cdot\eta} \left[\phi_1(\cdot;0) + \frac{\partial\phi_1}{\partial\eta_k}(\cdot;0)\eta_k + \frac{1}{2!}\frac{\partial^2\phi_1}{\partial\eta_k\partial\eta_\ell}(\cdot;0)\eta_k\eta_\ell\right] d\eta. \tag{5.6}$$

As mentioned earlier, either one can replace the first derivative of ϕ_1 by its explicit forms or determine it numerically from the first eigenvectors computed in the mesh points adjacent to the origin. In the same way, one can compute the second partial derivatives of ϕ_1 too. In particular, with the same eigenvectors used for the determination of $\partial\phi_1/\partial\eta_k$, one can calculate the second derivative in the case of symmetric periodic cells. More precisely, one uses a second-order finite difference formula to obtain the second derivatives of

$\phi_1(\cdot;0)$ (see Section 6.2.2 for more details), then its value at the origin is known explicitly from Theorem 2.1 and with the eigenvectors at the adjacent points to the origin one can easily determine this term, without any additional computational cost.

We will see later in Section 6.2.2 that the first-order approximation of θ^ε performs very similar to the classical first-order corrector term and the second-order approximation $\tilde{\theta}^\varepsilon_{(2)}$ produces almost the same result as the Bloch approximation function θ^ε and far better than the first-order classical corrector.

Remark 5.1. The Bloch wave method described above is more suitable for parallel computers. More precisely, we have to determine the first eigenvalue $\lambda_1(\eta)$ and the first eigenvector $\phi_1(\cdot;\eta)$ of the generalized eigenvalue problem (3.10) in a small ad hoc grid around the origin $(0,0)$ in Y'. But the eigenvalue problems are independent for each $\eta \in Y'$. This independence allows to use parallel computers for the determination of the eigenvalues, eigenvectors and consequently one can reduce the computation time.

6. Numerical examples

In this section, we present exhaustive numerical examples supporting our earlier claims in this paper. More precisely, we applied the above methods to both one and two-dimensional problems. First, we compare the homogenized coefficients and the auxiliary functions χ_k obtained by both methods, and then we deal with the classical first- and second-order correctors. Finally, we make a comparative study between the Bloch approximation function θ^ε and their Taylor approximations with the classical first-order corrector.

6.1. Two-dimensional case

6.1.1. Comparison of homogenized coefficients and functions χ_k by classical and Bloch methods

Example 6.1. Consider the representative cell as given in Fig. 1 with

$$\begin{cases} a_{k\ell 0} = \delta_{k\ell} \text{ (the Kronecker's index)} & \text{in } Y_0, \\ a_{k\ell 1} = \lambda\delta_{k\ell} & \text{in } Y_1, \end{cases}$$

where $a_{k\ell 0}$ and $a_{k\ell 1}$ represent the coefficients belonging to the regions Y_0 and Y_1, respectively.

In order to determine the homogenized coefficients, we have to solve (2.6) with the coefficients as given above. Here, we solve the above equation for five different values of λ, $(1000, 10, 1/18, 1/114, 1/1000)$ which arise from the physical problem of torsion of fiber-reinforced bars as studied by Bourgat and Lanchon [7].

In order to predict the accuracy of the Bloch method, we have applied it for different number of finite elements in the domain $Y =]0, 2\pi[^2$. The computed homogenized coefficients are given in Tables 1 and 2, respectively for $\lambda = 10$ and $1/18$.

In a first glance, one can imagine that the Bloch method needs the computations of many cell eigenvalue problems for different values of η. This is not exactly the real situation, because the homogenized coefficients are obtained from the Hessian of λ_1 at the origin. In order to obtain an accurate approximation of the Hessian, we have to use a very simple finite difference formula containing only a few grid points around the origin. More precisely, to determine $q_{k\ell}$ by the classical method a system of two elliptic PDEs have to be solved, in the Bloch method one has to solve two cell eigenvalue problems in the symmetric periodic cell case, whereas six eigenvalue problems in the non-symmetric periodic cell case. Here we utilize the symmetric property of the problem with respect to η, and make the calculations in only one side of the domain. Then,

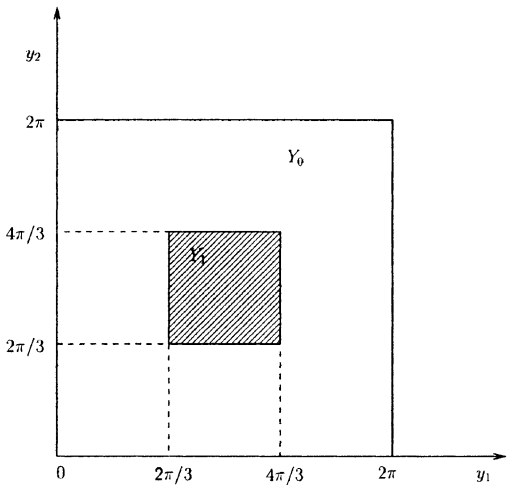

Fig. 1. Square representative cell Y.

Table 1
Homogenized coefficients for $\lambda = 10$

No. of elements	Bloch method (q_{11})	Classical method (q_{11})	Error
288	1.22490061044764	1.22490060876042	1.6872e−09
648	1.21947541934180	1.21947541576959	3.5722e−09
1152	1.21809582502003	1.21809583037969	2.5895e−09
1800	1.21585526726769	1.21585527835938	1.1092e−08

Table 2
Homogenized coefficients for $\lambda = 1/18$

No. of elements	Bloch method (q_{11})	Classical method (q_{11})	Error
288	0.81776545330035	0.81776545245266	8.4769e−10
648	0.81357789343615	0.81357789226366	1.1725e−09
1152	0.81170785322255	0.81170785128808	1.9345e−09
1800	0.81068319516579	0.81068319469725	4.6854e−10

by using a fourth-order centered difference formula we determine $q_{k\ell}$. For a function $f(x,y)$, the fourth-order finite difference formula for its second partial derivatives are given by:

$$\frac{\partial^2 f}{\partial x^2} = \frac{1}{12h^2}[-f_{i+2,j} + 16f_{i+1,j} - 30f_{i,j} + 16f_{i-1,j} - f_{i-2,j}],$$

$$\frac{\partial^2 f}{\partial x \partial y} = \frac{1}{144h^2}[(f_{i-2,j-1} - f_{i+2,j-2} - f_{i-2,j+2} + f_{i+2,j+2}) - 8(f_{i-1,j-2} - f_{i+1,j-2} - f_{i-1,j+2} + f_{i+1,j+2}) - 8(f_{i-2,j-1} - f_{i+2,j-1} - f_{i-2,j+1} + f_{i+2,j+1}) + 64(f_{i-1,j-1} - f_{i+1,j-1} - f_{i-1,j+1} + f_{i+1,j+1})],$$

$$\frac{\partial^2 f}{\partial y^2} = \frac{1}{12h^2}[-f_{i,j+2} + 16f_{i,j+1} - 30f_{i,j} + 16f_{i,j-1} - f_{i,j-2}],$$

Table 3
Homogenized coefficients for the stiff case

λ	Bloch method (q_{11})	Classical method (q_{11})	Error
10^3	1.28346598635829	1.28346598933957	2.9813e−09
10^{-3}	0.78981742620378	0.78982093144148	3.5052e−06

where $f_{i,j} = f(x_i, y_j)$. The above fourth-order formula is for the general case. The symmetry with respect to η significantly reduce the number of determination of λ_1. In the periodic cells case, one can enjoy the symmetry of y too.

To show that the accuracy between the classical and Bloch methods in the contrast of λ (stiff case), we performed the test for several values of λ as well as for various number of finite elements in the square periodic cell as given in Fig. 1 and presented the results in Table 3. From these results one can conclude that the accuracy is independent of the contrast of λ.

Remark 6.2. The CPU time is almost the same for both classical and Bloch methods in the symmetric periodic cell case and for the non-symmetric periodic cell case the Bloch method takes little more CPU time than the classical one. Further, the CPU time is not an important factor in the calculation of the $q_{k\ell}$, which are obtained almost in a real time computation.

Example 6.3. In this example, we state an interesting property of the homogenized coefficients. If the coefficients $a_{k\ell}$ are such that

$$\begin{cases} a_{kk} \text{ is symmetric with respect to the middle hyper planes} \\ \Delta_i (i = 1, \ldots, N) \text{ of the representative cell (see Fig. 2),} \end{cases} \tag{6.1}$$

then we have the following result:

$$q_{k\ell} = 0 \quad \text{for } k \neq \ell. \tag{6.2}$$

If we consider the representative cell as given in Fig. 3 with

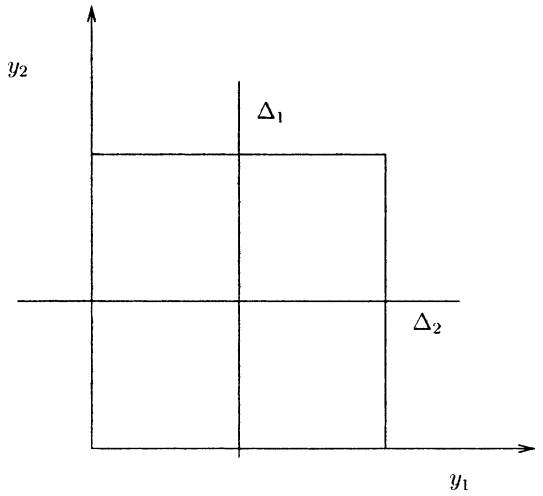

Fig. 2. Symmetric representative cell with respect to the middle hyper planes.

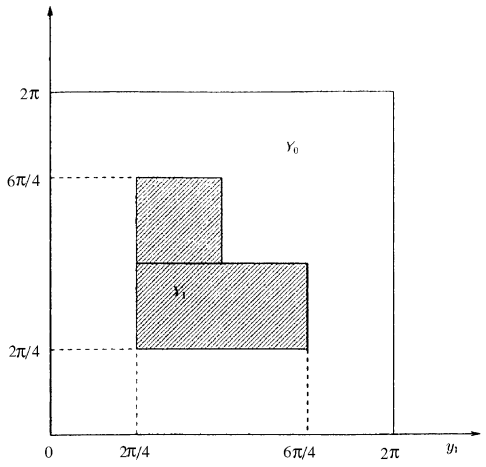

Fig. 3. Non-symmetric representative cell.

$$a_{k\ell} = \begin{cases} \delta_{k\ell} & \text{in } Y_0, \\ \lambda\delta_{k\ell} & \text{in } Y_1, \end{cases}$$

then, the assumption as given in (6.1) is not fulfilled. The homogenized coefficients obtained are not satisfy the result as given in (6.2), i.e., $q_{k\ell} \neq 0$ for $k \neq \ell$. The homogenized coefficients obtained by the classical and Bloch methods are given in Tables 4 and 5 respectively for $\lambda = 10$, $1/114$. Therefore, an heterogeneous medium made of two isotropic materials can be homogenized into an effective non-isotropic medium which is a well known fact among mathematicians and engineers.

Example 6.4. Let us consider the rhombus representative cell as given in Fig. 4 with the coefficients $a_{k\ell}$ as defined in Example 6.3.

Table 4
Homogenized coefficients for $\lambda = 10$

No. of elements	Bloch method		Classical method	
	$q_{11} = q_{22}$	$q_{12} = q_{21}$	$q_{11} = q_{22}$	$q_{12} = q_{21}$
288	1.4407055686	−0.0530067090	1.4407055683	−0.0530067077
512	1.4338541675	−0.0529771794	1.4338541611	−0.0529771805
800	1.4301258470	−0.0529388604	1.4301258453	−0.0529388584
1152	1.4278362419	−0.0529059499	1.4278362455	−0.0529059519

Table 5
Homogenized coefficients for $\lambda = 1/114$

No. of elements	Bloch method		Classical method	
	$q_{11} = q_{22}$	$q_{12} = q_{21}$	$q_{11} = q_{22}$	$q_{12} = q_{21}$
288	0.6513966796	−0.0427392436	0.6513966483	−0.0427392262
512	0.6467155635	−0.0427134690	0.6467155279	−0.0427134497
800	0.6441183367	−0.0426752552	0.6441182991	−0.0426752343
1152	0.6424950912	−0.0426422131	0.6424950540	−0.0426421954

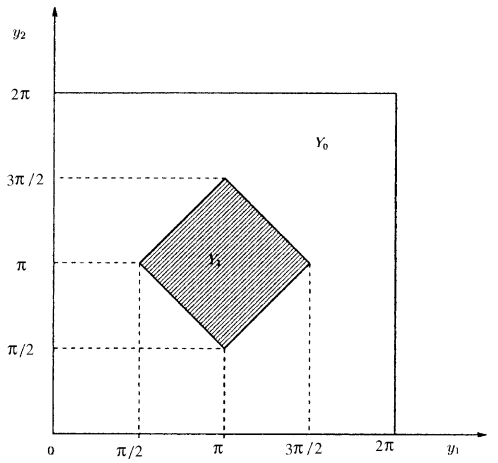

Fig. 4. Rhombus representative cell.

In this example, we consider a different shape of the periodic cell which is given in Fig. 4. Here, the shape of Y_1 is a rhombus instead of a square as considered in Example 6.1. The triangulation is made such that the discontinuities of the coefficients $a_{k\ell}$ coincide with the sides of the triangles. Tables 6 and 7 show the homogenized coefficients obtained by the classical and Bloch methods respectively for $\lambda = 1/18, 1/114$.

Remark 6.5. From the numerical results presented in Tables 1–7, one can find out the accuracy of the Bloch method in comparison with the classical one. The homogenized coefficients obtained by the Bloch and classical methods coincide with at most eight digits. Further, from the above numerical results, one can notice that the homogenized coefficients strongly depend on the chosen shape of Y_1.

From the above test problems we verified that the formula as given in (2.15) produces more than eight digits accurate results for the homogenized coefficients obtained from the classical formula (2.9). Further, we found that the formulas for χ_k as given in (2.16) produces the same results as the classical one defined to be the solution of the problem (2.6). For this, we have applied it to all the above test problems and predicted that both coincide up to eight digits accuracy. In Fig. 5 we show χ_1, χ_2 obtained by both the classical (χ_1, χ_2 defined to be the solutions of (2.6)) by solid line and Bloch methods (χ_1, χ_2 defined to be the left hand

Table 6
Homogenized coefficients for $\lambda = 1/18$

No. of elements	Bloch method (q_{11})	Classical method (q_{11})	Error
512	0.79242012651417	0.79242012579792	7.1625e−10
1152	0.78910981068346	0.78910980779788	2.8856e−09

Table 7
Homogenized coefficients for $\lambda = 1/114$

No. of elements	Bloch method (q_{11})	Classical method (q_{11})	Error
512	0.77233355955759	0.77233350607510	5.3482e−08
1152	0.76820226431582	0.76820220708207	5.7234e−08

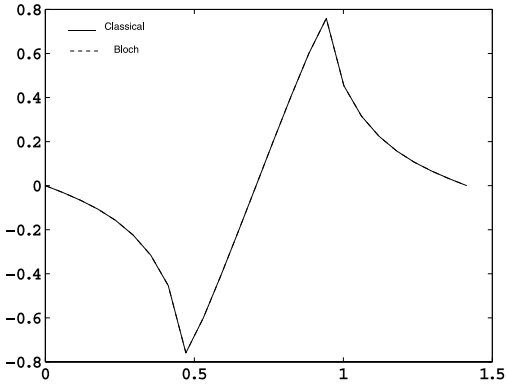

Fig. 5. Comparison of χ_k's obtained by classical and Bloch methods for the non-symmetric representative cell as given in Fig. 3 for $\lambda = 1/18$.

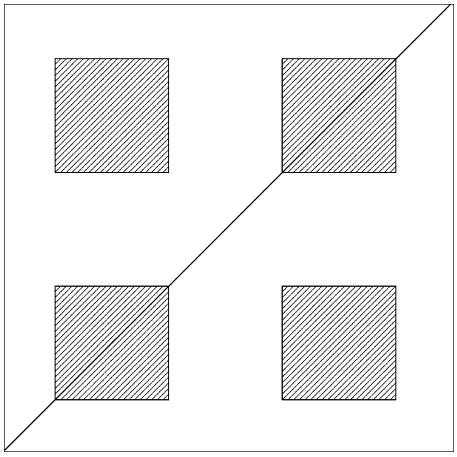

Fig. 6. Diagonal section.

side in (2.16)) by dot-line restricted along the diagonal $y_2 = y_1$ of Y as indicated in Fig. 6 (since both perfectly coincide, it is not easy to distinguish them in the plots).

6.1.2. Homogenized solution

Example 6.6. Consider the following boundary value problems. Let u^ε and u^* be respectively the solutions of the following problems:

$$\begin{cases} A^\varepsilon u^\varepsilon = f & \text{in } \Omega, \\ u^\varepsilon = 0 & \text{on } \partial\Omega \end{cases} \tag{6.3}$$

and

$$\begin{cases} -q_{k\ell}\dfrac{\partial^2 u^*}{\partial x_k \partial x_\ell} = f & \text{in } \Omega, \\ u^* = 0 & \text{on } \partial\Omega. \end{cases} \tag{6.4}$$

Let us consider a representative cell similar to the one as given in Fig. 1 with $Y =]0,1[^2$ instead of $]0,2\pi[^2$ and

$$a_{k\ell} = \begin{cases} \delta_{k\ell} & \text{in } Y_0, \\ \lambda\delta_{k\ell} & \text{in } Y_1. \end{cases}$$

In this example, we take $\Omega =]0,1[^2$; $f = 10, \varepsilon = 1/2,\ 1/4,\ 1/8$, and $\lambda = 10,\ 1/18,\ 1/144$.

This model situation occurs in the study of torsion of a cylindrical elastic bar with reinforcing fibres. The region Y_1 indicates the cross-section of a fibre and Y_0 that of the "matrix". The elastic constants are thus different in two regions. By $\varepsilon \to 0$ it is meant that the number of periodically distributed reinforcing fibres is steadily increased but the ratio of the volume occupied by the fibres to that occupied by the matrix is kept constant, for example, in this case, it is $1/9$ (see [7]).

The homogenized solution which is the solution of a second-order elliptic equation with constant coefficients (6.4) is obtained without any difficulty. On the other hand the computation of u^ε needs a triangulation which must be very fine as ε becomes small. We now examine the convergence of u^ε towards u^*. It is well known that

$$u^\varepsilon \rightharpoonup u^* \quad \text{in } H_0^1(\Omega) \text{ (weakly)}$$

and, if the coefficients $a_{k\ell}$ are sufficiently smooth (see [4]) one has

$$\|u^\varepsilon - u^*\|_{C^0(\overline{\Omega})} \leqslant C\varepsilon.$$

In this section, we show numerical results on the convergence of u^ε towards u^* and the figures presented are representations of the solutions u^ε and u^* restricted along a diagonal of Ω as indicated in Fig. 6. One can see in Figs. 7–10 that u^ε converges towards u^* as $\varepsilon \to 0$ but also that the difference between u^ε and u^* becomes greater whenever $\lambda < 1$. In Figs. 7–10, red and blue colors respectively stand for the exact and homogenized solutions. Moreover, we have indicated in Tables 8–10 the error $(u^\varepsilon - u^*)$ in the norms of spaces $L^\infty(\Omega)$, $L^2(\Omega)$, and $H_0^1(\Omega)$, respectively for $\lambda = 10,\ 1/18,\ 1/114$.

Remark 6.7. From the numerical errors given in Tables 8–10, we see that $\|u^\varepsilon - u^*\|_{H_0^1(\Omega)}$ does not converge but $\|u^\varepsilon - u^*\|_{L^2(\Omega)}$ and $\|u^\varepsilon - u^*\|_{L^\infty(\Omega)}$ converge to zero as we can see in Figs. 7–10. We also find that the values of $\sup_\Omega |u^\varepsilon - u^*|$ have a linear decrease as $\varepsilon \to 0$ though the coefficients $a_{k\ell}$ are discontinuous.

6.1.3. First-order corrector

Let us denote by v_1^ε the corrected solution obtained by the first-order corrector term, that is,

$$v_1^\varepsilon = u^* + \varepsilon u_1^\varepsilon.$$

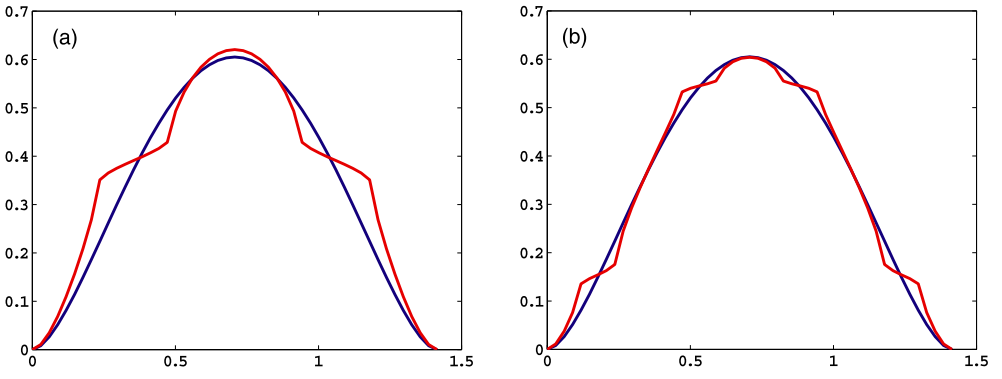

Fig. 7. Comparison of u^ε with u^* for (a) $\lambda = 10$, $\varepsilon = 1/2$ and (b) $\lambda = 10$, $\varepsilon = 1/4$.

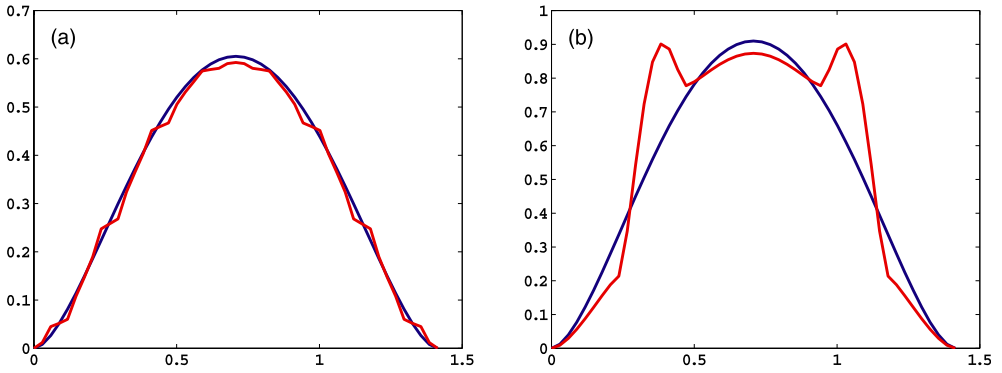

Fig. 8. Comparison of u^{ε} with u^{*} for (a) $\lambda = 10$, $\varepsilon = 1/8$ and (b) $\lambda = 1/18$, $\varepsilon = 1/2$.

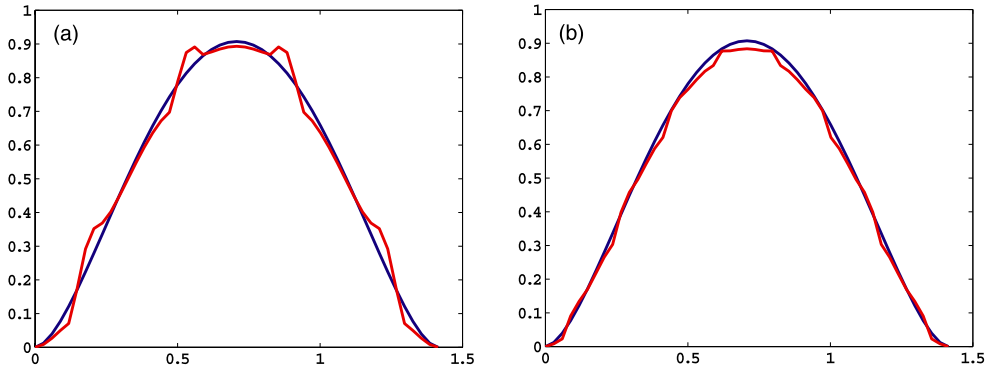

Fig. 9. Comparison of u^{ε} with u^{*} for (a) $\lambda = 1/18$, $\varepsilon = 1/4$ and (b) $\lambda = 1/18$, $\varepsilon = 1/4$.

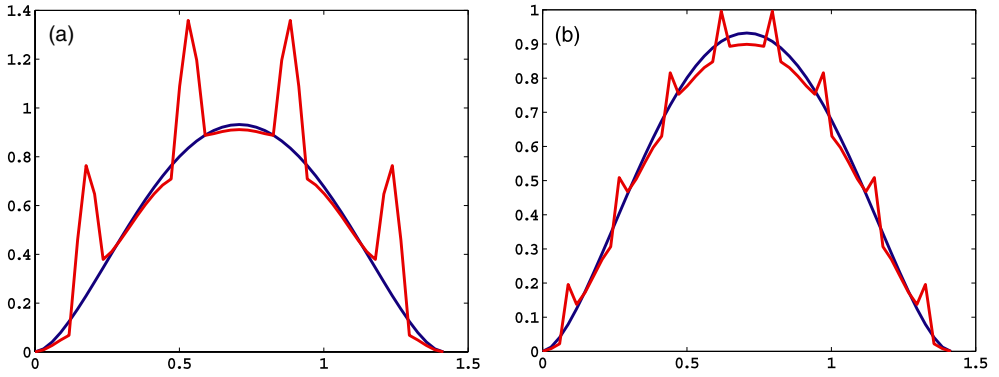

Fig. 10. Comparison of u^{ε} with u^{*} for (a) $\lambda = 1/144$, $\varepsilon = 1/4$ and (b) $\lambda = 1/144$, $\varepsilon = 1/8$.

Let us consider the case $\lambda = 10$ in the problem as given in Example 6.6. Here, we add the first-order periodic corrector to the homogenized solution in order to improve the rate of convergence. The partial derivatives

Table 8
Convergence of the error $(u^\varepsilon - u^*)$ for $\lambda = 10$

ε	$\sup_\Omega \lvert u^\varepsilon - u^*\rvert$	$\frac{\lVert u^\varepsilon - u^*\rVert_{L^2(\Omega)}}{\lVert u^*\rVert_{L^2(\Omega)}}$	$\frac{\lVert u^\varepsilon - u^*\rVert_{H_0^1(\Omega)}}{\lVert u^*\rVert_{H_0^1(\Omega)}}$
1/2	0.1249	0.1169	0.3249
1/4	0.0682	0.0599	0.3684
1/8	0.0396	0.0299	0.3858

Table 9
Convergence of the error $(u^\varepsilon - u^*)$ for $\lambda = 1/18$

ε	$\sup_\Omega \lvert u^\varepsilon - u^*\rvert$	$\frac{\lVert u^\varepsilon - u^*\rVert_{L^2(\Omega)}}{\lVert u^*\rVert_{L^2(\Omega)}}$	$\frac{\lVert u^\varepsilon - u^*\rVert_{H_0^1(\Omega)}}{\lVert u^*\rVert_{H_0^1(\Omega)}}$
1/2	0.2536	0.1131	0.3721
1/4	0.0979	0.0482	0.2738
1/8	0.0585	0.0228	0.2790

Table 10
Convergence of the error $(u^\varepsilon - u^*)$ for $\lambda = 1/114$

ε	$\sup_\Omega \lvert u^\varepsilon - u^*\rvert$	$\frac{\lVert u^\varepsilon - u^*\rVert_{L^2(\Omega)}}{\lVert u^*\rVert_{L^2(\Omega)}}$	$\frac{\lVert u^\varepsilon - u^*\rVert_{H_0^1(\Omega)}}{\lVert u^*\rVert_{H_0^1(\Omega)}}$
1/2	1.1955	0.4822	3.1637
1/4	0.4780	0.1299	1.5059
1/8	0.1195	0.0401	0.7243

of the homogenized solution, first-order corrector and the exact solution restricted along the diagonal of Ω are plotted respectively in blue, black and red colors in Fig. 11(a) and (b).

One can see in Fig. 11(a) that the first-order corrector gives a good approximation to the slopes of the partial derivatives of u^ε (that is, to its second-order partial derivatives). Also one can notice from Fig. 11(b) that the first-order periodic corrector does not give any correction to the peaks. Tables 11–13 show the error $(u^\varepsilon - v_1^\varepsilon)$ in the norms of spaces $L^\infty(\Omega)$, $L^2(\Omega)$ and $H_0^1(\Omega)$.

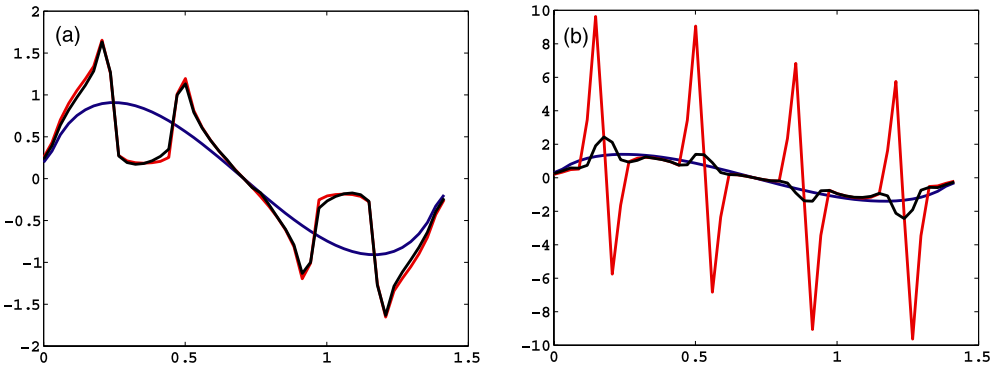

Fig. 11. The partial derivative of u^ε, u^*, v_1^ε for (a) $\lambda = 10$, $\varepsilon = 1/2$ and (b) $\lambda = 1/144$, $\varepsilon = 1/4$.

Table 11
Convergence of the error $(u^\varepsilon - v_1^\varepsilon)$ for $\lambda = 10$

ε	$\sup_\Omega \lvert u^\varepsilon - v_1^\varepsilon\rvert$	$\frac{\lVert u^\varepsilon - v_1^\varepsilon\rVert_{L^2(\Omega)}}{\lVert v_1^\varepsilon\rVert_{L^2(\Omega)}}$	$\frac{\lVert u^\varepsilon - v_1^\varepsilon\rVert_{H_0^1(\Omega)}}{\lVert v_1^\varepsilon\rVert_{H_0^1(\Omega)}}$
1/2	0.0539	0.0334	0.0775
1/4	0.0303	0.0132	0.0629
1/8	0.0225	0.0042	0.0486

Table 12
Convergence of the error $(u^\varepsilon - v_1^\varepsilon)$ for $\lambda = 1/18$

ε	$\sup_\Omega \lvert u^\varepsilon - v_1^\varepsilon\rvert$	$\frac{\lVert u^\varepsilon - v_1^\varepsilon\rVert_{L^2(\Omega)}}{\lVert v_1^\varepsilon\rVert_{L^2(\Omega)}}$	$\frac{\lVert u^\varepsilon - v_1^\varepsilon\rVert_{H_0^1(\Omega)}}{\lVert v_1^\varepsilon\rVert_{H_0^1(\Omega)}}$
1/2	0.2531	0.0710	0.4343
1/4	0.0625	0.0202	0.1840
1/8	0.0198	0.0057	0.0900

Table 13
Convergence of the error $(u^\varepsilon - v_1^\varepsilon)$ for $\lambda = 1/114$

ε	$\sup_\Omega \lvert u^\varepsilon - v_1^\varepsilon\rvert$	$\frac{\lVert u^\varepsilon - v_1^\varepsilon\rVert_{L^2(\Omega)}}{\lVert v_1^\varepsilon\rVert_{L^2(\Omega)}}$	$\frac{\lVert u^\varepsilon - v_1^\varepsilon\rVert_{H_0^1(\Omega)}}{\lVert v_1^\varepsilon\rVert_{H_0^1(\Omega)}}$
1/2	1.1955	0.4645	3.2657
1/4	0.4780	0.1135	1.5408
1/8	0.1195	0.0283	0.7595

6.1.4. Second-order corrector

Let v_2^ε be the corrected solution obtained with the first- and second-order correctors given by

$$v_2^\varepsilon = u^* + \varepsilon u_1^\varepsilon + \varepsilon^2 u_2^\varepsilon.$$

Here also we consider the same problem as given in Example 6.6. Fig. 12 shows the partial derivatives of the solutions u^ε, u^*, v_1^ε and v_2^ε for $\lambda = 1/114$, $\varepsilon = 1/4$. Here blue, rose, black (dot-lines) and red colors respectively denote the partial derivatives of u^*, v_1^ε, v_2^ε and u^ε restricted along the diagonal of Ω. Actually, the second-order corrector provides better approximation to the exact solution u^ε it is difficult to distinguish both of them in the plot as given in Fig. 12. The partial derivatives of v_2^ε (black dot-line) is exactly plotted on the partial derivatives of u^ε (red solid line).

If we compare Figs. 11(b) and 12, we see that the second-order periodic corrector gives the correction of the peaks of the partial derivatives of u^ε in the case $\lambda < 1$.

The error $(u^\varepsilon - v_2^\varepsilon)$ is presented in Tables 14 and 15. One can compare these results with those of Tables 12 and 13 to see the effect of the second-order correctors in the energy norm (H^1-strong convergence). We note from Table 15 that the results obtained for $\varepsilon = 1/8$ are worse than those obtained for $\varepsilon = 1/4$. This is due to the error made in the computation of u^ε, that is, we use only eight triangles in Y_1 (the region mentioned in the periodic cell in Fig. 1), which is not enough to capture the original behavior of u^ε there. Therefore, if $\lambda < 1$ and ε is small, even if the direct computation of u^ε is possible, homogenization gives better results in a symmetric context.

Remark 6.8. In the stiff cases (when $\lambda = 10^3$ or 10^{-3}), there is a boundary layer which arises from the boundary condition and becomes more and more complicate for the numerical study. These results in the loss of accuracy for both first- and second-order correctors. This interesting phenomena is under study in our forthcoming paper [9].

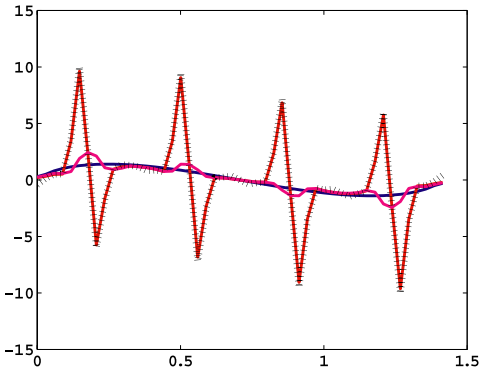

Fig. 12. The partial derivative of u^ε, u^*, v_1^ε, v_2^ε for $\lambda = 1/114$, $\varepsilon = 1/4$.

Table 14
Convergence of the error $(u^\varepsilon - v_2^\varepsilon)$ for $\lambda = 1/18$

ε	$\sup_\Omega \lvert u^\varepsilon - v_2^\varepsilon\rvert$	$\frac{\lVert u^\varepsilon - v_2^\varepsilon\rVert_{L^2(\Omega)}}{\lVert v_2^\varepsilon\rVert_{L^2(\Omega)}}$	$\frac{\lVert u^\varepsilon - v_2^\varepsilon\rVert_{H_0^1(\Omega)}}{\lVert v_2^\varepsilon\rVert_{H_0^1(\Omega)}}$
1/2	0.0548	0.0500	0.0729
1/4	0.0531	0.0107	0.0637
1/8	0.0312	0.0027	0.0447

Table 15
Convergence of the error $(u^\varepsilon - v_2^\varepsilon)$ for $\lambda = 1/114$

ε	$\sup_\Omega \lvert u^\varepsilon - v_2^\varepsilon\rvert$	$\frac{\lVert u^\varepsilon - v_2^\varepsilon\rVert_{L^2(\Omega)}}{\lVert v_2^\varepsilon\rVert_{L^2(\Omega)}}$	$\frac{\lVert u^\varepsilon - v_2^\varepsilon\rVert_{H_0^1(\Omega)}}{\lVert v_2^\varepsilon\rVert_{H_0^1(\Omega)}}$
1/2	0.0605	0.0504	0.1242
1/4	0.0583	0.0123	0.0368
1/8	0.0342	0.0031	0.0375

6.2. One-dimensional case

The purpose of this section is to present the numerical accuracy of the Bloch approximation function θ^ε and its Taylor approximations to u^ε and the classical first-order corrector. To simplify matters, we consider the one-dimensional problems for illustration. We apply the Bloch approximation for both the smooth and discontinuous coefficient cases. The examples are given below.

Example 6.9 (The discontinuous coefficients case). Consider the following problem:

$$\begin{cases} -\dfrac{\mathrm{d}}{\mathrm{d}x}\left(a\left(\dfrac{x}{\varepsilon}\right)\dfrac{\mathrm{d}u^\varepsilon}{\mathrm{d}x}(x)\right) + u^\varepsilon(x) = f(x), \quad x \in \Omega =]-2\pi, 2\pi[, \\ u^\varepsilon(-2\pi) = 0, \quad u^\varepsilon(2\pi) = 0, \end{cases} \tag{6.5}$$

where $a(x/\varepsilon)$ is the oscillating coefficient and $f(x) = \sin(x)/x$. In this example the coefficient $a(y)$ for $y \in Y =]0, 2\pi[$ is defined as

$$a(y) = \begin{cases} \lambda & \text{in } Y_1 \overset{\text{def}}{=} \left(\dfrac{2\pi}{3}, \dfrac{4\pi}{3}\right) \\ 1 & \text{in } Y_0 \overset{\text{def}}{=} Y \setminus Y_1. \end{cases}$$

We consider two different values for λ as $\lambda = 1/18$ and $1/114$ which were obtained from physical applications for the two-dimensional case in [6].

Example 6.10 (The continuous coefficient case). Consider the problem as given in Example 6.9 with the following smooth coefficients

$$a(y) = 2 + \cos(y) \quad \text{or} \quad a(y) = 2 + \sin(y).$$

6.2.1. Comparison of θ^ε with u^ε and the first-order corrector

In this section, we make a comparative study between the Bloch approximation function θ^ε, the exact solution u^ε, and the classical first-order corrector term v_1^ε defined by

$$v_1^\varepsilon(x) = u^*(x) + \varepsilon\chi\left(\frac{x}{\varepsilon}\right)\frac{\mathrm{d}u^*}{\mathrm{d}x}(x),$$

where u^* is the homogenized solution and $\chi = \chi_k$ corresponds to the one-dimensional version of χ_k.

To check the accuracy of θ^ε, we applied it to different values of λ in the discontinuous coefficients case and also for the continuous coefficients for several number of finite elements in the domain Ω. For the computation of θ^ε, we determine the first eigenvalue $\phi_1(\cdot;\eta)$ of the generalized eigenvalue problem discretized by 48 and 96 points in the periodic cell $Y =]0, 2\pi[$ for $\eta \in Y' = [-1/2, 1/2]$. We divide the domain Y' into 80 and 160 points. We recall that the eigenvectors are independent of ε and it is enough to determine it once and store for the calculations of different values of ε. From these results, we have selected a few and plotted θ^ε, u^ε and v_1^ε respectively in blue, red and black colors in Figs. 13 and 14. These figures plot θ^ε, u^ε and v_1^ε, inside a peak which was obtained by zooming in small different intervals around the origin. From these plots one can easily identify that the Bloch approximation θ^ε is more closer to u^ε than the classical first-order corrector v_1^ε which reflects our claim in Section 5.

Further, we have indicated in Tables 16 and 17 the errors $(u^\varepsilon - \theta^\varepsilon)$, $(u^\varepsilon - v_1^\varepsilon)$ and $(\theta^\varepsilon - v_1^\varepsilon)$ in the norms of the spaces $L^2(\omega)$ and $H^1(\omega)$, where $\omega = [-\pi, \pi]$. Here, we have compared these differences only in ω instead of the full domain $\Omega =]-2\pi, 2\pi[$. This is because the Bloch approximation function θ^ε is theoretically valid in the absence of boundaries. Therefore, a fair comparison between θ^ε and v_1^ε should consist in comparing a local norm or semi-norm for $(u^\varepsilon - \theta^\varepsilon)$ and $(u^\varepsilon - v_1^\varepsilon)$, and this has been done by computing the above norm/

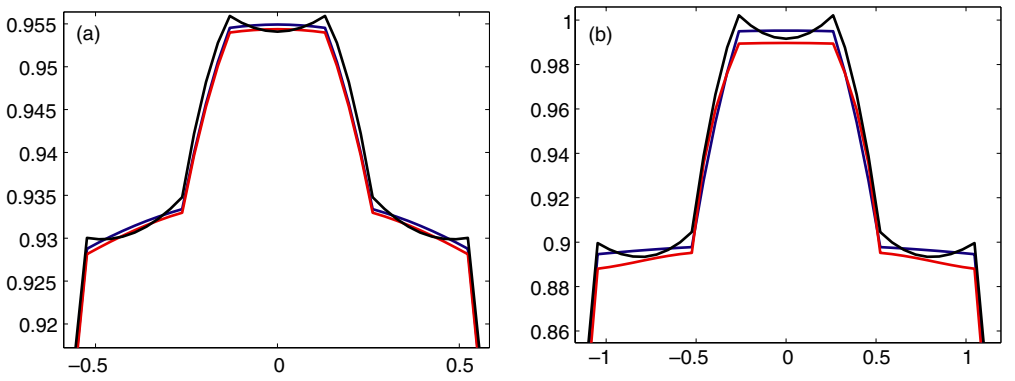

Fig. 13. Plots of u^ε, θ^ε and v_1^ε (Example 6.9) for (a) $\lambda = 1/18$, $\varepsilon = 1/16$ and (b) $\lambda = 1/144$, $\varepsilon = 1/8$.

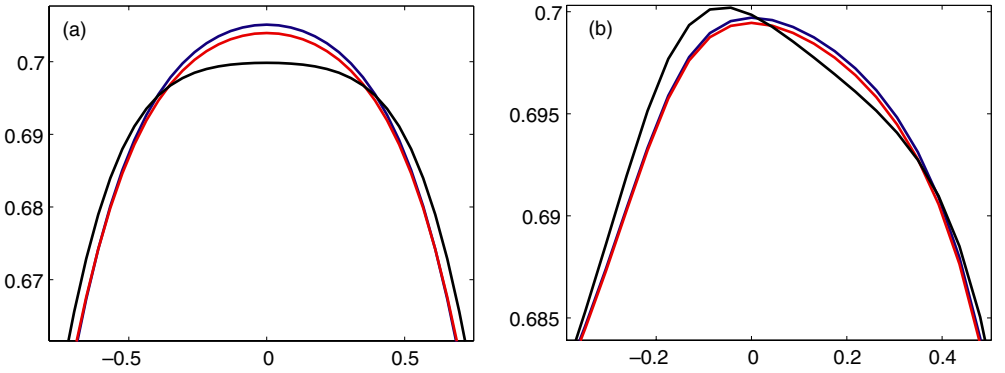

Fig. 14. Plots of u^ε, θ^ε and v_1^ε (Example 6.10) for (a) $a(y) = 2 + \cos(y)$, $\varepsilon = 1/4$ and (b) $a(y) = 2 + \sin(y)$, $\varepsilon = 1/8$.

Table 16
Convergence of the errors for $\lambda = 1/18$ (Example 6.9)

ε	$\frac{\|u^\varepsilon - \theta^\varepsilon\|_{L^2(\omega)}}{\|u^\varepsilon\|_{L^2(\omega)}}$	$\frac{\|u^\varepsilon - v_1^\varepsilon\|_{L^2(\omega)}}{\|u^\varepsilon\|_{L^2(\omega)}}$	$\frac{\|\theta^\varepsilon - v_1^\varepsilon\|_{L^2(\omega)}}{\|u^\varepsilon\|_{L^2(\omega)}}$	$\frac{\|u^\varepsilon - \theta^\varepsilon\|_{H^1(\omega)}}{\|u^\varepsilon\|_{H^1(\omega)}}$	$\frac{\|u^\varepsilon - v_1^\varepsilon\|_{H^1(\omega)}}{\|u^\varepsilon\|_{H^1(\omega)}}$	$\frac{\|\theta^\varepsilon - v_1^\varepsilon\|_{H^1(\omega)}}{\|u^\varepsilon\|_{H^1(\omega)}}$
1/2	0.1724	0.1560	0.0761	0.4691	0.5269	0.2268
1/4	0.0280	0.0282	0.0224	0.1619	0.1670	0.1084
1/8	0.0037	0.0063	0.0052	0.0400	0.0563	0.0480
1/16	6.2142e−04	0.0016	0.0013	0.0098	0.0253	0.0235
1/32	1.2833e−04	3.9213e−04	3.2160e−04	0.0025	0.0121	0.0116
1/64	2.8916e−05	9.7805e−05	8.2675e−05	6.2251e−04	0.0059	0.0057
1/128	1.2331e−05	2.4456e−05	2.5430e−05	1.5841e−04	0.0029	0.0029

Table 17
Convergence of the errors for Example 6.10

ε	$\frac{\|u^\varepsilon - \theta^\varepsilon\|_{L^2(\omega)}}{\|u^\varepsilon\|_{L^2(\omega)}}$	$\frac{\|u^\varepsilon - v_1^\varepsilon\|_{L^2(\omega)}}{\|u^\varepsilon\|_{L^2(\omega)}}$	$\frac{\|\theta^\varepsilon - v_1^\varepsilon\|_{L^2(\omega)}}{\|u^\varepsilon\|_{L^2(\omega)}}$	$\frac{\|u^\varepsilon - \theta^\varepsilon\|_{H^1(\omega)}}{\|u^\varepsilon\|_{H^1(\omega)}}$	$\frac{\|u^\varepsilon - v_1^\varepsilon\|_{H^1(\omega)}}{\|u^\varepsilon\|_{H^1(\omega)}}$	$\frac{\|\theta^\varepsilon - v_1^\varepsilon\|_{H^1(\omega)}}{\|u^\varepsilon\|_{H^1(\omega)}}$
1/2	0.0454	0.0148	0.0470	0.1407	0.0956	0.1321
1/4	0.0029	0.0047	0.0062	0.0250	0.0462	0.0524
1/8	4.4291e−04	0.0013	0.0013	0.0057	0.0224	0.0235
1/16	9.2924e−05	3.3298e−04	3.3210e−04	0.0017	0.0119	0.0120
1/32	9.0173e−05	1.1839e−04	1.1907e−04	0.0010	0.0062	0.0061
1/64	9.0708e−05	8.0293e−05	8.9194e−05	0.0010	0.0032	0.0031

semi-norm in a compactly supported domain ω in Ω. In addition, the above mentioned errors are also presented inside the main peak of u^ε. They are denoted by $(\cdot)$ in Table 18. Here, the above norm/semi-norm measures the relative errors in a variable local sub-domain which depends on ε (in fact, it decreases as $\varepsilon \to 0$).

Apart from the comparison of the accuracy between the Bloch function and the classical first-order corrector to the exact solution, we determine the CPU time for each of these two terms. Here, we exclude the CPU time for the computations of the auxiliary function χ (in the classical method) and the first eigenvector $\phi_1(\cdot;\eta)$ (in the Bloch method) and the computed CPU times are given in Table 19 (in seconds). The number of mesh points used in the domain $[-2\pi, 2\pi]$ for each case is $24/\varepsilon$. This is mainly because to

Table 18
Convergence of the errors for $\lambda = 1/114$ inside a peak (Example 6.9)

ε	$\frac{\|u^\varepsilon - \theta^\varepsilon\|_{L^2(\cdot)}}{\|u^\varepsilon\|_{L^2(\cdot)}}$	$\frac{\|u^\varepsilon - v_1^\varepsilon\|_{L^2(\cdot)}}{\|u^\varepsilon\|_{L^2(\cdot)}}$	$\frac{\|\theta^\varepsilon - v_1^\varepsilon\|_{L^2(\cdot)}}{\|u^\varepsilon\|_{L^2(\cdot)}}$	$\frac{\|u^\varepsilon - \theta^\varepsilon\|_{H^1(\cdot)}}{\|u^\varepsilon\|_{H^1(\cdot)}}$	$\frac{\|u^\varepsilon - v_1^\varepsilon\|_{H^1(\cdot)}}{\|u^\varepsilon\|_{H^1(\cdot)}}$	$\frac{\|\theta^\varepsilon - v_1^\varepsilon\|_{H^1(\cdot)}}{\|u^\varepsilon\|_{H^1(\cdot)}}$
1/2	0.1236	0.1641	0.0771	0.7088	0.9154	0.4080
1/4	0.0277	0.0365	0.0277	0.7951	0.8082	0.4597
1/8	0.0051	0.0084	0.0068	0.2894	0.3713	0.3336
1/16	0.0013	0.0022	0.0017	0.0460	0.2533	0.2888
1/32	2.0441e−04	5.7547e−04	4.5110e−04	0.0258	0.2362	0.2413
1/64	4.0874e−05	1.3370e−04	1.0832e−04	0.0070	0.2573	0.2473
1/128	6.4592e−07	4.1580e−05	4.1012e−05	8.6563e−04	0.4704	0.4685

Table 19
CPU time (in seconds) for the Classical and Bloch methods

ε	Classical method	Bloch method
1/2	0.0455	0.6086
1/4	0.0810	1.1532
1/8	0.1687	2.3392
1/16	0.3852	4.4615
1/32	1.0117	9.1412
1/64	3.0656	18.2195
1/128	10.6353	37.3967

handle the discontinuous coefficients $a(x/\varepsilon)$ in the numerical calculation of u^ε. From this table one can notice that the difference between both methods is significant for bigger values of ε, whereas it starts to decrease as $\varepsilon \to 0$, which is really the interesting case. The computations are carried out in a Pentium III processor machine with 64 MB RAM and 500 MHz speed by using MATLAB.

6.2.2. Comparison of the Taylor approximations of θ^ε with u^ε and v_l^ε

This section reports a comparative analysis between the Taylor approximation functions $\tilde{\theta}^\varepsilon_{(1)}$ and $\tilde{\theta}^\varepsilon_{(2)}$ of θ^ε, the exact solution u^ε, and the classical first-order corrector v_1^ε in terms of figures and numerical tables.

For the calculation of $\tilde{\theta}^\varepsilon_{(1)}$, we determine the first Bloch mode at $\eta = -0.005$, 0.005 and using a second-order finite difference formula we compute the first derivative of ϕ_1. We made a wide variety of comparisons between all these terms and presented some selected results for the readers. As mentioned earlier the first-order Taylor approximation function $\tilde{\theta}^\varepsilon_{(1)}$ provides almost the same approximate value as the first-order corrector term v_1^ε to u^ε. So it is difficult to distinguish between both $\tilde{\theta}^\varepsilon_{(1)}$ and v_1^ε in the plots. In order to make it easy to the readers, the solution and the *difference* between both functions are plotted in Fig. 15. In Fig. 15(a) the blue, red, black (dot-line) respectively stand for $\tilde{\theta}^\varepsilon_{(1)}, u^\varepsilon$ and v_1^ε. The black dot-line v_1^ε is exactly on the blue solid line $\tilde{\theta}^\varepsilon_{(1)}$. The error is plotted in Fig. 15(b). Further, we have compared both functions with u^ε in different local norms and presented the relative errors in Tables 20 and 21.

By using the two eigenvalues as determined for the function $\tilde{\theta}^\varepsilon_{(1)}$ and the value of $\phi_1(\cdot;0) = 1/\sqrt{2\pi}$ we determine its second derivate which is used in the approximation function $\tilde{\theta}^\varepsilon_{(2)}$. To compare the second-order Taylor approximation function $\tilde{\theta}^\varepsilon_{(2)}$ with the exact solution and the classical first-order corrector, as usual we performed several numerical tests for different values of λ in the discontinuous coefficients case, and the continuous coefficients case. From these results, we conclude that $\tilde{\theta}^\varepsilon_{(2)}$ gives a better approximation to the exact solution u^ε than the classical first-order corrector v_1^ε as well as $\tilde{\theta}^\varepsilon_{(1)}$. The error between the partial derivatives of the exact solution and the first- and second-order Taylor approximation functions are plotted

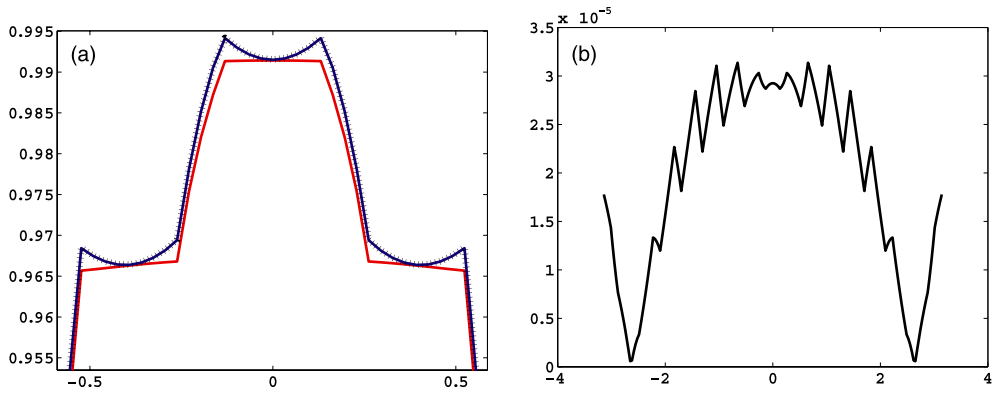

Fig. 15. For $\lambda = 1/114$ and $\varepsilon = 1/8$ (Example 6.9). Plot of (a) u^ε, $\tilde{\theta}^\varepsilon_{(1)}$ and v^ε_1 and (b) the difference $|\tilde{\theta}^\varepsilon_{(1)} - v^\varepsilon_1|$.

Table 20
Convergence of the errors for $\lambda = 1/18$ (Example 6.9)

ε	$\frac{\|u^\varepsilon - \tilde{\theta}^\varepsilon_{(1)}\|_{L^2(\omega)}}{\|u^\varepsilon\|_{L^2(\omega)}}$	$\frac{\|u^\varepsilon - v^\varepsilon_1\|_{L^2(\omega)}}{\|u^\varepsilon\|_{L^2(\omega)}}$	$\frac{\|\tilde{\theta}^\varepsilon_{(1)} - v^\varepsilon_1\|_{L^2(\omega)}}{\|u^\varepsilon\|_{L^2(\omega)}}$	$\frac{\|u^\varepsilon - \tilde{\theta}^\varepsilon_{(1)}\|_{H^1(\omega)}}{\|u^\varepsilon\|_{H^1(\omega)}}$	$\frac{\|u^\varepsilon - v^\varepsilon_1\|_{H^1(\omega)}}{\|u^\varepsilon\|_{H^1(\omega)}}$	$\frac{\|\tilde{\theta}^\varepsilon_{(1)} - v^\varepsilon_1\|_{H^1(\omega)}}{\|u^\varepsilon\|_{H^1(\omega)}}$
1/2	0.1560	0.1560	4.5212e−05	0.5270	0.5269	1.2364e−04
1/4	0.0282	0.0282	4.9738e−05	0.1671	0.1670	9.4410e−05
1/8	0.0062	0.0063	4.8679e−05	0.0563	0.0563	8.9808e−05
1/16	0.0016	0.0016	1.5296e−05	0.0253	0.0253	2.9192e−05
1/32	3.8831e−04	3.9213e−04	1.3413e−05	0.0121	0.0121	2.7509e−05
1/64	9.4968e−05	9.7805e−05	1.3193e−05	0.0059	0.0059	2.7486e−05
1/128	2.4568e−05	2.4456e−05	1.3002e−05	0.0029	0.0029	2.7657e−05

Table 21
Convergence of the errors for Example 6.10

ε	$\frac{\|u^\varepsilon - \tilde{\theta}^\varepsilon_{(1)}\|_{L^2(\omega)}}{\|u^\varepsilon\|_{L^2(\omega)}}$	$\frac{\|u^\varepsilon - v^\varepsilon_1\|_{L^2(\omega)}}{\|u^\varepsilon\|_{L^2(\omega)}}$	$\frac{\|\tilde{\theta}^\varepsilon_{(1)} - v^\varepsilon_1\|_{L^2(\omega)}}{\|u^\varepsilon\|_{L^2(\omega)}}$	$\frac{\|u^\varepsilon - \tilde{\theta}^\varepsilon_{(1)}\|_{H^1(\omega)}}{\|u^\varepsilon\|_{H^1(\omega)}}$	$\frac{\|u^\varepsilon - v^\varepsilon_1\|_{H^1(\omega)}}{\|u^\varepsilon\|_{H^1(\omega)}}$	$\frac{\|\tilde{\theta}^\varepsilon_{(1)} - v^\varepsilon_1\|_{H^1(\omega)}}{\|u^\varepsilon\|_{H^1(\omega)}}$
1/2	0.0148	0.0148	1.0264e−04	0.0958	0.0956	1.0522e−04
1/4	0.0047	0.0047	9.7128e−05	0.0461	0.0462	1.2175e−04
1/8	0.0013	0.0013	9.5238e−05	0.0225	0.0224	1.2706e−04
1/16	3.2466e−04	3.2410e−04	8.6594e−05	0.0119	0.0120	1.3339e−04
1/32	1.2558e−04	1.1839e−04	8.6315e−05	0.0061	0.0062	1.3406e−04
1/64	9.4903e−05	8.0293e−05	8.6207e−05	0.0032	0.0032	1.3431e−04

in Fig. 16(a) and (b). The difference between the partial derivatives of u^ε and the first-order corrector v^ε_1 is very similar to the plot as given in Fig. 16(a). As usual the compared errors in different norms are provided in Tables 22 and 23.

With these above numerical experiments one can easily conclude the facts mentioned earlier in this paper namely, that (i) the Bloch approximation function θ^ε produces better approximations for the exact solution u^ε than the first-order corrector v^ε_1 at least in the smooth coefficient case, and provide a similar approximation as v^ε_1 in the discontinuous case, (ii) the first-order Taylor approximation function $\tilde{\theta}^\varepsilon_{(1)}$ performs in a very similar way as v^ε_1, and (iii) the second-order Taylor approximation function $\tilde{\theta}^\varepsilon_{(2)}$ gives a

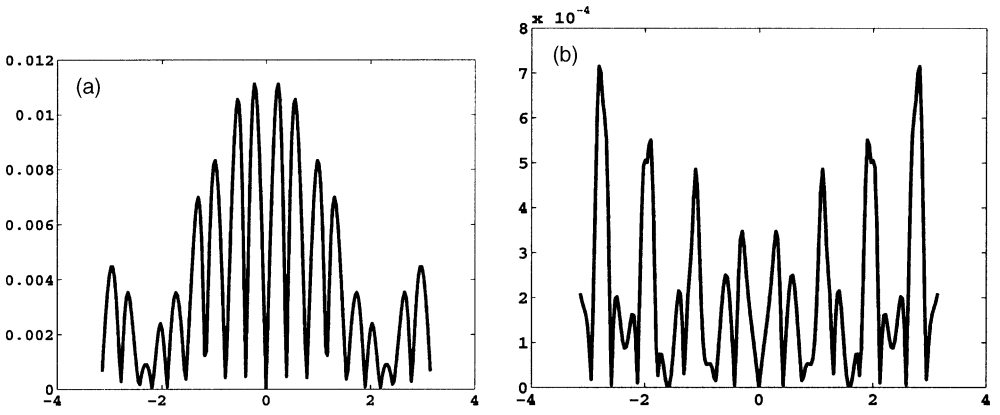

Fig. 16. For $a(y) = 2 + \cos(y)$ and $\varepsilon = 1/8$ (Example 6.9). Plot of (a) $|\frac{du^\varepsilon}{dx} - \frac{d\tilde{\theta}^\varepsilon_{(1)}}{dx}|$ and (b) $|\frac{du^\varepsilon}{dx} - \frac{d\tilde{\theta}^\varepsilon_{(2)}}{dx}|$.

Table 22
Convergence of the errors for $\lambda = 1/114$ (Example 6.9)

ε	$\frac{\|u^\varepsilon - \tilde{\theta}^\varepsilon_{(2)}\|_{L^2(\omega)}}{\|u^\varepsilon\|_{L^2(\omega)}}$	$\frac{\|u^\varepsilon - \tilde{\theta}^\varepsilon_{(1)}\|_{L^2(\omega)}}{\|u^\varepsilon\|_{L^2(\omega)}}$	$\frac{\|\tilde{\theta}^\varepsilon_{(2)} - v^\varepsilon_1\|_{L^2(\omega)}}{\|u^\varepsilon\|_{L^2(\omega)}}$	$\frac{\|u^\varepsilon - \tilde{\theta}^\varepsilon_{(2)}\|_{H^1(\omega)}}{\|u^\varepsilon\|_{H^1(\omega)}}$	$\frac{\|u^\varepsilon - \tilde{\theta}^\varepsilon_{(1)}\|_{H^1(\omega)}}{\|u^\varepsilon\|_{H^1(\omega)}}$	$\frac{\|\tilde{\theta}^\varepsilon_{(2)} - v^\varepsilon_1\|_{H^1(\omega)}}{\|u^\varepsilon\|_{H^1(\omega)}}$
1/2	0.2100	0.2198	0.0750	0.6350	0.7741	0.2075
1/4	0.0501	0.0498	0.0250	0.4044	0.3941	0.1053
1/8	0.0085	0.0098	0.0063	0.1493	0.1437	0.0504
1/16	0.0012	0.0022	0.0016	0.0391	0.0478	0.0235
1/32	2.0991e−04	5.1461e−04	3.9362e−04	0.0088	0.0166	0.0117
1/64	3.8435e−05	1.1998e−04	1.0064e−04	0.0022	0.0068	0.0059
1/128	1.4163e−05	2.7089e−05	2.9802e−05	6.3216e−04	0.0031	0.0030

Table 23
Convergence of the errors for Example 6.10

ε	$\frac{\|u^\varepsilon - \tilde{\theta}^\varepsilon_{(2)}\|_{L^2(\omega)}}{\|u^\varepsilon\|_{L^2(\omega)}}$	$\frac{\|u^\varepsilon - \tilde{\theta}^\varepsilon_{(1)}\|_{L^2(\omega)}}{\|u^\varepsilon\|_{L^2(\omega)}}$	$\frac{\|\tilde{\theta}^\varepsilon_{(2)} - v^\varepsilon_1\|_{L^2(\omega)}}{\|u^\varepsilon\|_{L^2(\omega)}}$	$\frac{\|u^\varepsilon - \tilde{\theta}^\varepsilon_{(2)}\|_{H^1(\omega)}}{\|u^\varepsilon\|_{H^1(\omega)}}$	$\frac{\|u^\varepsilon - \tilde{\theta}^\varepsilon_{(1)}\|_{H^1(\omega)}}{\|u^\varepsilon\|_{H^1(\omega)}}$	$\frac{\|\tilde{\theta}^\varepsilon_{(2)} - v^\varepsilon_1\|_{H^1(\omega)}}{\|u^\varepsilon\|_{H^1(\omega)}}$
1/2	0.0097	0.0148	0.0184	0.0305	0.0958	0.0960
1/4	6.3622e−04	0.0047	0.0050	0.0056	0.0461	0.0478
1/8	1.9503e−04	0.0013	0.0013	0.0013	0.0255	0.0231
1/16	7.2026e−05	3.2466e−04	3.2802e−04	5.6092e−04	0.0119	0.0121
1/32	9.0001e−05	1.2558e−04	1.1884e−04	9.9506e−04	0.0061	0.0061
1/64	9.0702e−05	9.4903e−05	1.3505e−04	0.0010	0.0032	0.0031

better approximation to the exact solution u^ε, without further computational cost from the calculation of $\tilde{\theta}^\varepsilon_{(1)}$.

Remark 6.11. In all the tables corresponding to the one-dimensional examples we have given the error only up to $\varepsilon = 1/128$ except in the smooth coefficient case (Example 6.10) where we were not able to go up to this threshold and merely treat $\varepsilon = 1/64$. This is because the coefficients are variables here and the oscillations in the exact solution u^ε could not be capture for $\varepsilon < 1/128$. The round off error increases abruptly for small values of ε in the calculation of u^ε.

7. Discussion

Two numerical methods are reported in this paper to solve elliptic PDEs with rapidly oscillating coefficients. The first method is based on the asymptotic approximation, which includes the determination of the homogenized solution, the classical first- and second-order correctors, numerically. To obtain an approximate solution to the multi-scale problems, one has to solve the homogenized equation and to improve the accuracy and the rate of convergence, it is essential to add classical correctors. We have computed all these terms numerically by using the classical approach in our first method. In addition to that we have used the Bloch approach to determine the homogenized coefficients, and some auxiliary functions appear in the calculation. The accuracy of both methods are compared for different kinds of problems. From the numerical examples one can see that the homogenization method is an effective one to solve these types of problems when the number of cells is large.

The second method consists of determining an oscillating integral involving the homogenized coefficients, the classical Fourier transform of the right hand side function f and the first eigenvector $\phi_1(\cdot;\eta)$ of the generalized Sylvester's type eigenvalue problem. This Bloch approximation function provides better approximations to u^ε than the classical first-order corrector in the smooth coefficients case. In addition, we have provided first- and second-order Taylor approximations of θ^ε. The numerical implementation of these two terms are much easier than the Bloch approximation function and provides better approximations to the exact solution. An issue which can be seen as a merit of the Bloch method over the classical one is the fact that the former method is better adapted to parallel computation. Because the computations of the eigenvalue $\lambda_1(\cdot)$ and eigenvector $\phi_1(\cdot;\eta)$ are independent for each $\eta \in Y'$. Moreover, since they are independent of ε, the calculation needs only to be done once for ever in the computation of θ^ε.

Acknowledgements

This work has been partially supported by FONDAP through its Programme on Mathematical-Mechanics. The authors gratefully acknowledge the Chilean and French Governments through the Scientific Committee Ecos-Conicyt.

The authors express their sincere thanks to the referees whose incisive comments allowed us not only to improve the presentation of our numerical results but also to strengthen and add a section to the earlier version of the paper.

References

[1] M. Avellaneda, L. Berlyand, J.-F. Clouet, Frequency-dependent acoustics of composites with interfaces, SIAM J. Appl. Math. 60 (2000) 2143–2181.
[2] M. Avellaneda, T. Hou, G. Papanicolaou, Finite difference approximations for partial differential equations with rapidly oscillating coefficients, Math. Modell. Numer. Anal. 25 (1991) 693–710.
[3] J. Bear, Use of models in decision making, in: T. Dracos, F. Stauffer (Eds.), Transport and Reactive Process in Aquifers, Balkema, Rotterdam, 1994, pp. 3–9.
[4] A. Bensoussan, J.-L. Lions, G. Papanicolaou, Asymptotic Analysis for Periodic Structures, North-Holland, Amsterdam, 1978.
[5] F. Bloch, Über die quantenmechanik der electronen in kristallgittern, Z. Phys. 52 (1928) 555–600.
[6] J. Bourgat, Numerical experiments of the homogenization method for operators with periodic coefficients, Technical Report 277, Institut de Recherche d'Informatique et d'Automatique, Le Chesnay, France, 1978.
[7] J. Bourgat, H. Lanchon, Application of the homogenization method to composite materials with periodic structures, Technical Report 208, Institut de Recherche d'Informatique et d'Automatique, Le Chesnay, France, 1976.
[8] Y. Capdeboscq, Homogenization of a diffusion equation with drift, C.R. Acad. Sci. Paris Série I 327 (1998) 807–812.
[9] C. Conca, S. Natesan, M. Vanninathan, Numerical experiments with the Bloch–Floquet approach in homogenization, Working Paper, 2002.

[10] C. Conca, R. Orive, M. Vanninathan, Bloch approximation in homogenization and applications, SIAM J. Math. Anal. 33 (2002) 1166–1198.
[11] C. Conca, J. Planchard, M. Vanninathan, Fluids and Periodic Structures, No. 38 in Research in Applied Mathematics, John Wiley/Masson, New York/Paris, 1995.
[12] C. Conca, M. Vanninathan, Homogenization of periodic structures via Bloch decomposition, SIAM J. Appl. Math. 57 (1997) 1639–1659.
[13] T. Hou, X. Wu, A multiscale finite element method for elliptic problems in composite materials and porous media, J. Comput. Phys. 134 (1997) 169–189.
[14] S. Kesavan, Homogenization of elliptic eigenvalue problems: Part 2, Appl. Math. Optim. 5 (1979) 197–216.
[15] J.-L. Lions, Some Methods in the Mathematical Analysis of Systems and Their Control, Gordon and Breach, Beijing, New York, 1981.
[16] A. Matache, I. Babuška, C. Schwab, Generalized *p*-fem in homogenization, Numer. Math. 86 (2000) 319–375.
[17] R. Morgan, I. Babuška, An approach for constructing families of homogenized equations for periodic media I: Integral representation and its consequences, SIAM J. Math. Anal. 22 (1991) 1–15.
[18] J. Planchard, Méthodes Mathématiques en Neutronique, Collection de la Direction des Études et Recherches dÉDF, Eyrolles, Paris, 1995.
[19] E. Sánchez-Palencia, Non-Homogeneous Media and Vibration Theory, Lecture Notes in Physics, vol. 127, Springer-Verlag, Berlin, 1980.
[20] M. Vanninathan, Homogenization and eigenvalue problems in perforated domains, Proc. Indian Acad. Sci. Math. Sci. 90 (1981) 239–271.